Title
I. RELAXATIONS IN A MOLECULAR CRYSTAL II. THE FERMI MOMENTUM OF ALUMINUM FROM 0 TO 100 KILOBARS

Author
Burton, James J.

Publication Date
1967-04-01

UCRL-17479

University of California

Ernest O. Lawrence Radiation Laboratory

I. RELAXATIONS IN A MOLECULAR CRYSTAL

II. THE FERMI MOMENTUM OF ALUMINUM FROM 0 TO 100 KILOBARS

Berkeley, California

DISCLAIMER

UCRL-17479

UNIVERSITY OF CALIFORNIA

Lawrence Radiation Laboratory
Berkeley, California

AEC Contract No. W-7405-eng-48

I. RELAXATIONS IN A MOLECULAR CRYSTAL
II. THE FERMI MOMENTUM OF ALUMINUM FROM 0 TO 100 KILOBARS

James J. Burton

(Ph. D. Thesis)

April 1967

CONTENTS

---

[1] Published in J. Phys. Chem. Solids, 27, 961 (1966) by the author and G. Jura.

[2] To be published in J. Phys. Chem. Solids, by the author and G. Jura.

[3] To be published in J. Phys. Chem., by the author and G. Jura.

[4] Presented at the Symposium on Fundamentals of Gas-Surface Interactions, December 14, 1966, San Diego, California, by the author and G. Jura.

I. RELAXATIONS IN A MOLECULAR CRYSTAL
II. THE FERMI MOMENTUM OF ALUMINUM FROM 0 TO 100 KILOBARS

James J. Burton

Inorganic Materials Research Division, Lawrence Radiation Laboratory,
and Department of Chemistry, University of California,
Berkeley, California

ABSTRACT

April 1967

Properties of imperfect lattices of monatomic face centered cubic crystals are examined theoretically. The atomic interactions are represented by pair-wise additive potentials. The configuration of the atoms near each imperfection are obtained. The effects of relaxations on the energies of the defects are examined.

For bulk defects — vacancies, divacancies, substitutional atoms, and substitutional atom-vacancy pairs — the relaxations are small and only slightly alter the energy of the defect. Vacancies in argon are bound to other vacancies or to substitutional impurities.

The activation energy, E, in the Arrhenius expression

$$D = D_o \, e^{-E/RT}$$

is calculated for self diffusion in argon for both monovacancy and divacancy exchange diffusion. The results for monovacancy mechanism (E = 3812 cal) and the divacancy mechanism (E = 4847 cal) are both in reasonable agreement with the experimental diffusion coefficient.

$$D = 15 \, e^{-4120 \text{ cal}/RT}$$

The frequency factor, D_o, for the divacancy mechanism is much greater than that for monovacancies. This indicates that the self diffusion mechanism

in solid argon at zero pressure may be via divacancies. The activation energies for neon and krypton impurity diffusion via monovacancy exchange are 2187 and 3733 cal, respectively. In all cases, the relaxations of surrounding atoms drastically lowered the barrier to diffusion.

The relaxations and surface energies of (100), (111), and (110) surfaces of aluminum, argon, calcium, copper, lead, nickel, and silver are calculated. The relaxations of the surface are less than 15% of the bulk planar spacing. The relaxations only slightly alter the surface energies.

The energies of adsorption of argon, krypton, and neon atoms on the (100) surface plane of argon are calculated. Relaxation appreciably affects the adsorption energies. The adsorption energies increase in the order neon, argon, krypton.

The Fermi momentum of aluminum is studied from 0 to 100 kilobars pressure. Bridgman anvils were used to generate the pressure and the positron annihilation spectrum was studied at five pressures. The Fermi momenta are obtained from the positron annihilation spectra. The experimental values of the Fermi momenta of aluminum are in excellent agreement with the prediction of the free electron model:

$$p_F = \hbar \left(\frac{3\pi^2 Z}{V} \right)^{1/3}$$

where Z is the number of conduction electrons per unit cell of the metal and V is the volume of the unit cell.

I. RELAXATIONS IN A MOLECULAR CRYSTAL

A. Introduction

A perfect single crystal is characterized by a basic building block, the unit cell, which is infinitely duplicated so as to fill all of space. The equilibrium configuration of a solid is that which minimizes its free energy. If the atoms in the solid are (initially) assumed to be at rest, the equilibrium configuration is that of minimum potential energy. When an atom is displaced slightly from its equilibrium position, a force acts on the atom to restore it to its equilibrium position. Early investigators of solids assumed simplified models of infinite solids and examined the vibrations of the atoms about their equilibrium positions. These workers, with their models, obtained heat capacities, entropies, and other thermodynamic data on simple solids;[1-3] their results were found to compare favorably with experimental data. Recently, with the advent of high speed computers, more complicated models of solids have been used and better agreement with experiment obtained.[4,5]

Unfortunately, solids in the real world are not infinite perfect single crystals. They have surfaces, vacant sites, grain boundaries, and contain impurities. These defects significantly affect the physical and chemical properties of real solids and must be considered in discussing the behavior of real solids.[6]

The effects of surfaces, vacancies, and impurities on the lattice vibrations have been examined.[7-10] It was found that these defects can drastically influence the vibrations of the atoms but that the perturbations decrease rapidly with distance from the defect.

When a defect is introduced into the model of a perfect infinite crystal, the remaining imperfect crystal may not be a minimum potential configuration unless some relaxation of the lattice occurs in the neighborhood of the defect. Finding the minimum potential configuration of a defective lattice requires a minimization of a complicated function in many variables. Early workers were forced to find closed mathematical expressions for the results and then to evaluate the expressions by hand; their work was, of necessity, restricted to simple problems.[11] Recently high speed computers have made it possible to deal with more complex problems as the computers can be programmed to search directly for the minimum potential configuration. Distortions of perfect lattices in the neighborhood of surfaces[12] and vacancies[13] have been examined in this way. In subsequent sections we shall examine the distortion of the perfect crystal around internal vacancies, divacancies, and impurity atoms (Sec. I-C), diffusion via single and divacancies (Sec. I-D), dilation of perfect surfaces (Sec. I-E) and of distortion near surface impurities and vacancies (Sec. I-F). We will find that though distortions of a face-centered cubic crystal in the neighborhood of a defect are usually numerically very small, the distortions can appreciably alter the energy of the defect and so must be considered in any attempt to understand the defect. In each problem treated we will develop an expressions for the energy of the defective lattice and then minimize that energy by allowing the lattice to relax in the region of the defect. All computations were carried out with the aid of IBM 7094 and CDC 6600 computers.

We will use argon as our prototype solid except in Secs. I-E and I-F where certain metals will also be examined. Theoretical calculations on argon afford many advantages over other solids. Argon is a monatomic molecular solid crystallizing in a face centered cubic lattice and has a short range potential. Ionic solids present many theoretical difficulties as it is not yet known how best to represent the polarization effects.[14] In metals one encounters the perturbation of the conduction electrons, a difficulty which has not yet been overcome. Solid argon presents neither of these obstacles. It is well known that the properties of argon may be reasonably represented by a two body potential function.[15] It is hoped that calculations based on a simplified model of argon will yield results of at least qualitative validity for argon and will give some insight into other simple solids, particularly other molecular crystals and face centered cubic metals.

B. Model

We adopt the following model of argon: (1) all quantum effects are neglected; (2) only the potential energy need be considered; (3) the total potential energy is pairwise additive; and (4) the atoms interact with a Lennard-Jones potential of the form

$$V(r) = \frac{\beta}{r^m} - \frac{\alpha}{r^6}$$

where r is the distance between the atoms. For most of our calculations we will use the parameters given by Kanzaki[15] with m = 12, which give the binding energy of solid argon to be 2035 cal/mole and the 0°K interatomic distance to be 3.79 Å. In Sec. I-C we will also carry out calculations with m = 7 as recent work by Alder and Van Thiel indicates that argon can best be represented by a 6-7 potential at very high pressures.[16]

These assumptions are open to question. (1) neglects zero point motion and (2) restricts the validity of the results to 0°K. The assumption of pairwise additivity of the potential (3) is most dubious. This model indicates that the hexagonal close packed form should be the stable phase of argon but argon experimentally is face centered cubic. Jansen[17] has shown that three body forces can explain the observed stability of face centered cubic argon and Sparnaay[18] has estimated that neglect of three body forces can introduce errors into energy computations of as much as 30%. Rossi and Danon[19] have found that inclusion of three body forces introduces a large error into predicted energies of vaporization: they attribute this error to either four body forces or a poor potential function. Bullough et al.[20] have concluded from a study of stacking faults in argon that many body forces contribute less than .4% of the total

binding energy. Alder[21] has shown that slight modifications of the Lennard-Jones 6-12 potential can lead to body centered cubic as the theoretically stable form of argon and has pointed out[22] that the Lennard-Jones potential may now show the correct shape of the true argon two body potential.

On the basis of the above assumptions the binding energy of the lattice may be written for m = 12 as

$$E_B = \frac{1}{2} N \sum_{i \neq j} V(rij)$$

$$= \frac{1}{2} N \left(\frac{\beta A_{12}}{r_o^{12}} - \frac{\alpha A_6}{r_o^6} \right)$$

where

$$A_n = \sum_{\text{lattice points}} \frac{1}{(x^2 + y^2 + z^2)^{1/2}}$$

and α and β are parameters in the pair potential function, r_o, is the solid interatomic distance, N is the number of atoms in the crystal, and the binding energy of the lattice E_B is the negative of the heat of sublimation E_S.

$$E_B = -E_S$$

The factor 1/2 occurs in the above expression so that each pair interaction is counted only once.

Following the work of Alder et al.,[12] the edge of the unit cell is made equal to 2, which places the restriction on the lattice points that the sum of the coordinates of a point must be even. With this restriction we have used the method of Lennard-Jones and Ingham[23] to calculate A_6

and A_{12} and have obtained

$$A_6 = 14.45392103$$

$$A_{12} = 12.13188018$$

which are in agreement with their earlier calculations.

C. Internal Vacancies, Divacancies and Substitutional Impurities

1. Introduction

Although some measurements have been made from which the energy of the formation of a vacancy can be deduced,[24] it has not been possible to deduce the distortions that occur in the immediate neighborhood of the vacancy. To date, the only internal defects which have been considered are the formation of vacancies in argon[25-29] and certain metals.[13] In this section, a more refined calculation is made for argon. In addition calculations are made for the substitution of an impurity atom in the lattice, for the formation of a vacancy next to the impurity atom, for the formation of two adjacent vacancies, and also for the effect of a change of interatomic distance on the energy of formation of the vacancy, and for the effect of a change in the potential function. This section will examine two of the more elementary lattice defect problems, namely perturbation of an infinite face centered cubic molecular crystal in the neighborhood of a vacancy of an impurity atom and the stability of di-defects in fcc molecular crystals. Presumably the results obtained here would apply qualitatively to other molecular crystals.

Several calculations of the energy of formation of a vacancy have been carried out in which the authors neglected kinetic effects. Girifalco and Streetman[30] carried out calculations on a bcc lattice, considering all points in a large box around the defect but neglecting distant neighbors. They found the nearest and next-nearest neighbors relaxing inwards and a large (20%) energy correction due to relaxation. Kanzaki[25] calculated relaxations around a vacancy in Ar (fcc) using a Lennard-Jones 6-10 potential. However, he assumed the effect of relaxation on the energy was second order in the relaxation and considered only nearest

and next-nearest neighbor interactions. He found that the nearest neighbors relaxed towards the vacancy and the next-nearest away, the relaxation of the next-nearest neighbors being greater than that of the nearest. Hall[26] also calculated the effect of a vacancy on a fcc lattice and assumed a second order relation between relaxation and energy. He found the nearest and next-next-nearest neighbors relax inwards towards the vacancy and the next-nearest relax outwards. His findings showed that the relaxations fall off rapidly with distance from the defect. Girifalco and Weizer[13] have calculated the distortion around a vacancy of a number of face centered cubic and body center cubic metals. They assumed that the distortions are radial and that the metals may be represented by a Morse pairwise additive potential. Girifalco and Weizer found that the nearest neighbors to the vacancy move inwards towards the vacant site, the next nearest outwards, and the third nearest inwards; their relaxations decreased rapidly with distance from the defect.

Glyde[27] has calculated the energy of formation of a vacancy in argon and has taken into account the temperature expansion of the lattice. He found that the energy of formation of a vacancy decreases with increasing temperature.

Nardelli and Repanai-Chiarotti[28] and Foreman and Lidiard[29] have carried out dynamical calculations based on the Einstein model. Nardelli's relaxations agree with those found here and his relaxation energy is much larger than that found considering only potential effects. Foreman also determined the energy of formation of a vacancy from heat capacity data for solid argon and found that the predicted relaxation energy was not large enough to account for the smallness of the energy of formation of a vacancy, which was 25% lower than expected.

Strip and Kirkwood[31] have calculated the interaction of separated vacancies and have found that they attract with a force whose potential varies as $1/r^6$ where r is the separation of the defects.

Johnson[32] has carried out static calculations on the stability of di-vacancies in metals and have found them to be stable in certain configurations.

Our calculations of the relaxations around a vacancy in a fcc lattice show that the nearest and next-next-nearest neighbors move towards the defect, and that the next-nearest move away. This is in accord with the latest calculations.[26] The correction in the energy of formation of the defect due to relaxation is small at zero pressure. In the present calculations the treatment is more general than in the earlier static results in that the calculations are not restricted by the assumption that only second order terms in the relaxation are significant and that distant neighbors may be neglected. Since the same, or essentially the same, treatment can be used when foreign atoms are present or for a compressed lattice, results are also presented for these calculations. We have also calculated the energy of formation of a vacancy next to another vacancy and next to a neon or krypton impurity. In all cases the energy required to produce the second vacancy is lower than that in the perfect lattice. Relaxations around the di-defects and energy corrections were small as in the case isolated defects.

2. Isolated Defects

a. Calculations. A vacancy is created in a solid by removing a single atom from the interior of the crystal to the surface. For such a process the energy of formation of vacancy, E_V°, if no relaxations occur, and

$$E_V^\circ = E_S$$

where E_S is the average energy of sublimation of the solid. With the model of argon adopted in Sec. I and a Lennard-Jones 6-12 potential

$$E_V^\circ = 2035 \text{ cal/mole of vacancies}$$

If the lattice is allowed to relax around the defect, the true energy of formation of the vacancy, E_V, is obtained by considering all potential pairs involving relaxing atoms

$$E_V = E_V^\circ + \Delta E$$

where ΔE is the change in the potential from the unrelaxed to the relaxed state.

The vacancy is assumed to be at (0,0,0). Assuming that only the nearest neighbors to the defect relax and that they relax radially and symmetrically, $(1,1,0) \rightarrow (1-\delta_1, 1-\delta_1, 0)$, the energy of a single nearest neighbor, with relaxation δ, is

$$\mathcal{E}(\underline{\delta}) = \sum_{\substack{x^2 + y^2 + z^2 = 2n \\ n > 1}} V(1-\delta_1-x,\ 1-\delta_1-y,\ z)$$

$$+ V(2-2\delta_1,\ 2-2\delta_1, 0) + 2V(2-2\delta_1, 0, 0) + 4V(1-\delta_1,\ 1-\delta_1, 0)$$

$$+ 4V(2-2\delta_1,\ 1-\delta_1,\ 1-\delta_1)$$

To simplify the calculations, the infinite sum is expanded as follows:

$$\mathcal{E}_1(\underline{\delta}) = \sum_{\substack{x^2 + y^2 + z^2 = 2n \\ n>1}} V(1-\delta_1-x,\ 1-\delta_1-xy,\ z)$$

$$= \sum_{\substack{x^2+y^2+z^2=2n \\ 2 \le n \le 16}} V(1-\delta_1-x,\ 1-\delta_1-y, z)$$

$$+ \sum_{\substack{x^2+y^2+z^2=2n \\ n > 16}} V(1-\delta_1-x,\ 1-\delta_1-y, z)$$

$$= \mathcal{E}_{11}(\delta_1) + \mathcal{E}_{12}(\delta_1)$$

$\mathcal{E}_{11}(\delta_1)$ is evaluated by direct summation while $\mathcal{E}_{12}(\delta_1)$ is obtained from a power series.

$$\begin{aligned}
\mathcal{E}_{12}(\underline{\delta}_1) = \; & -46.36 \\
& -17.90\{(\delta x)^2 + (\delta y)^2 + (\delta z)^2\} \\
& -13.20\{(\delta x)^4 + (\delta y)^4 + (\delta z)^4\} \\
& - .32\{(\delta x)^6 + (\delta y)^6 + (\delta z)^6\} \\
& - .04\{(\delta x)^8 + (\delta y)^8 + (\delta z)^8\} \\
& - 4.01\{(\delta x)^2(\delta y)^2 + (\delta x)^2(\delta z)^2 + (\delta y)^2(\delta z)^2\} \\
& - 8.84\{(\delta x)^4(\delta y)^2 + (\delta y)^4(\delta z)^2 \\
& \quad + (\delta x)^4(\delta z)^2 + (\delta z)^4(\delta x)^2 \\
& \quad + (\delta y)^4(\delta z)^2 + (\delta z)^4(\delta y)^2\} \\
& + 1.52\{(\delta x)^4(\delta y)^4 + (\delta x)^4(\delta z)^4 \\
& \quad + (\delta y)^4(\delta z)^4\} \\
& - .14\{(\delta x)^6(\delta y)^2 + (\delta y)^6(\delta x)^2 \\
& \quad + (\delta x)^6(\delta z)^2 + (\delta z)^6(\delta x)^2 \\
& \quad + (\delta y)^6(\delta z)^2 + (\delta z)^6(\delta y)^2 \\
& + 1.62\{(\delta x)^2(\delta y)^2(\delta z)^2\}
\end{aligned}$$

$$- 1.47\{(\delta x)^4(\delta y)^2(\delta z)^2 + (\delta x)^2(\delta y)^4(\delta z)^2 + (\delta x)^2(\delta y)^2(\delta z)^4\}$$

The power series expansion is used rather than an integral as integration will not yield as accurate an answer when the lower limit of integration is this small. The power series expansion given is for a point at (0,0,0) going to $(\delta x, \delta y, \delta z)$. It is not practical to expand

$$\mathcal{E}_1(\underline{\delta}) = \mathcal{E}_{11}(\underline{\delta}) + \mathcal{E}_{12}(\underline{\delta})$$

in a power series over all points because of the slowness with which such a series converges.

Summing over the twelve nearest neighbors, the expression for the energy is

$$\mathcal{E}(\underline{\delta}) = 6\{V(2-2\delta_1,\ 2-2\delta,\ 0) + 2V(2-2\delta_1,\ 0,0) + 4V\ (1-\delta_1,\ 1-\delta_1,\ 0) + 4V(2-2\delta_1,\ 1-\delta_1,\ 1-\delta_1)\} + 12\mathcal{E}_{11} + 12\mathcal{E}_{12}(\underline{\delta}).$$

Note that to obtain the total energy contribution of the twelve nearest neighbors, the interactions of the nearest neighbors with each other must be multiplied by six, not twelve, so that each pair is counted only once.

With this we may write

$$\Delta E(\underline{\delta}) = E(\underline{\delta}) - E(0)$$

where E is expanded as above.

If the nearest neighbors relax $(1,1,0) \rightarrow (1-\delta_1, 1-\delta_1, 0)$, the next-nearest $(2,0,0) \rightarrow (2-\delta_2, 0, 0)$ and the next-next-nearest $(1,1,2) \rightarrow (1-\delta_{31}, 1-\delta_{31}, 2-\delta_{32})$ then the energy of the relaxed lattice may be written as

$$E(\underline{\delta}) = \sum_{\substack{x^2+y^2+z^2=2n \\ n>3}}^{12} V(1-\delta_1, -x, 1-\delta_1-y, z)$$

$$+ \sum_{\substack{x^2+y^2+z^2=2n \\ n>3}}^{6} V(2-\delta_2-x, y, z)$$

$$+ \sum_{\substack{x^2+y^2+z^2=2n \\ n>3}}^{24} V(1-\delta_{31}-x, 1-\delta_{31}-y, 2-\delta_{32}-z)$$

$$+ 24V(1-\delta_2+\delta_1, 1-\delta_1, 0) + 24V(3-\delta_1-\delta_2, 1-\delta_1, 0)$$
$$+ 24V(1-\delta_1, 1-\delta_1, 2-\delta_2) + 48V(1-\delta_{32}+\delta_1, \delta_1-\delta_{31}, 1-\delta_{31})$$
$$+ 48V(3-\delta_1-\delta_{32}, \delta_1-\delta_{31}, 1-\delta_{31}) + 48V(1-\delta_{32}+\delta_1, 2-\delta_1-\delta_{31}, 1-\delta_{31})$$
$$+ 48V(3-\delta_1-\delta_{32}, 2-\delta_1-\delta_{31}, 1-\delta_{31}) + 24V(\delta_1-\delta_{31}, \delta_1-\delta_{31}, 2-\delta_{32})$$
$$+ 48V(2-\delta_{31}-\delta_1, \delta_1-\delta_3, 2-\delta_{32}) + 24V(2-\delta_{31}-\delta_1, 2-\delta_{31}-\delta_1, 2-\delta_{32})$$
$$+ 24V(\delta_2-\delta_{32}, 1-\delta_{31}, 1-\delta_{31}) + 24V(4-\delta_2-\delta_{32}, 1-\delta_{31}, 1-\delta_{31}, 1-\delta_{31})$$
$$+ 48V(2-\delta_{32}, 1-\delta_2+\delta_{31},) + 48V(2-\delta_{32}, 3-\delta_2-\delta_{31}, 1-\delta_{31})$$
$$+ 12V(4-2\delta_{32}, 0, 0) + 24V(4-2\delta_{32}, 2-2\delta_{31}, 0)$$
$$+ 12V(4-2\delta_{32}, 2-2\delta_{31}, 2-2\delta_{31}) + 24V(0, 2-2\delta_{31}, 0)$$
$$+ 12V(0, 2-2\delta_{31}, 2-2\delta_{31}) + 24V(1-\delta_{32}+\delta_{31}, 1-\delta_{32}+\delta_{31}, 0)$$
$$+ 24V(1-\delta_{32}+\delta_{31}, 1-\delta_{32}+\delta_{31}, 2-2\delta_{31}) + 48V(3-\delta_{32}-\delta_{31}, 1-\delta_{32}+\delta_{31}, 0)$$
$$+ 48V(3-\delta_{32}-\delta_{31}, 1-\delta_{32}+\delta_{31}, 2-2\delta_{31}) + 24V(3-\delta_{32}-\delta_{31}, 3-\delta_{32}-\delta_{31}, 2-2\delta_{31})$$
$$+ 24V(3-\delta_{32}-\delta_{31}, 3-\delta_{32}-\delta_{31}, 0) + 6V(2-2\delta_1, 2-2\delta_1, 0)$$
$$+ 12V(2-2\delta_1, 0, 0) + 24V(1-\delta_1, 1-\delta_1, 0)$$
$$+ 24V(2-2\delta_1, 7-\delta_1, 1-\delta_1) + 3V(4-2\delta_2, 0, 0)$$
$$+ 12V(2-\delta_2 2-\delta_2, 0)$$

Similar and obviously more complex expressions are written if more atoms are permitted to relax.

To minimize the energy, only ΔE need be considered since this is the only term in which the relaxations appear.

Minimization of ΔE was performed in a step wise manner. First the solution for the relaxation of the nearest neighbors was obtained. This was then the basis for the first approximation when the nearest and next-nearest neighbors were considered. The solution of this was then used as a starting point for the most complete calculations performed. The minimum for ΔE for each degree of relaxation examined was found by a half interval technique. Because of the machine time and labor required to carry the calculations to neighbors more distant from the defect and the qualitative significance of the results, computations were made only for the first three layers around the vacancy.

Calculations for an impurity atom are essentially the same as for a vacancy; this was done for a large and a small impurity atom. For these the constants used for argon

$$r_o = 3.79 \text{ A}$$
$$E_S = 2035 \text{ cal/mole}$$

were modified. Ar-Kr and Ar-Ne pair potentials were related to the 6-12 potentials of Ar,[15] Ne,[15] and Kr[33] in the following way. If r_{A-A} represents the gas equilibrium distance and U_{A-A} the depth of the well in the gas

$$r_{A-B} = \frac{r_{A-A} + r_{B-B}}{2}$$

$$U_{A-B} = \left(U_{A-A}\, U_{B-B}\right)^{1/2}$$

and r_{A-B} and U_{A-B} were used as parameters in the Lennard-Jones 6-12 potential.

b. Results. Calculations for the relaxation of the nearest neighbors was initially carried out assuming that the relaxation would preserve the xy, xz, and yz planes as planes of C_{4v} symmetry. This involves six independent variables and it was found, with this condition, that E_V is minimized by a relaxation which preserves the octahedral symmetry about the defect. Calculations for completely independent relaxation of the twelve nearest neighbors, a thirty-six variable problem, were not performed.

For the next- and next-next-nearest neighbors it was assumed that the relaxations would also have the high symmetry established for the nearest neighbors.

Those relaxations minimizing ΔE, and ΔE are given in Tables I-VIII. Relaxations are expressed in terms of the coordinates. The lattice point with coordinates (x,y,z) relative to the defect at 0,0,0) was relaxed to the new position (x-δy, y-δy, z-δz) and δx, xy, and δz are tabulated beneath x, y, and z. ΔE is given for each relaxation.

In each case the energy of formation of the defect in the unrelaxed lattice, E^O_D is given. E^O_D is the difference in energy between the perfect argon lattice and the defective (unrelaxed) lattice. For a Kr impurity energy is released on substitution of the impurity atom for the AR atom, and the effect of the relaxation is to increase the amount of energy released. Creation of a vacancy or substitution of a Ne for an AR atom requires energy and the relaxation decreases the amount required.

Table I. Configuration and energy of an isolated vacancy with $r/r_o = 1$, using a 6-12 potential. The vacancy is located at (0,0,0) and the relaxations of the neighbors are tabulated.

$E_D^0 = 2035$ cal/mole

(1,	1,	0)	(2,	0	0)	(2,	1,	1)	ΔE
6.055×10^{-3}	6.055×10^{-3}	0	-	-	-	-	-	-	-23.5 cal/mole
6.055×10^{-3}	6.055×10^{-3}	0	-3.412×10^{-3}	0	0	-	-	-	-25.5
6.420×10^{-3}	6.420×10^{-3}	0	-3.433×10^{-3}	0	0	8.80×10^{-4}	5.39×10^{-4}	5.39×10^{-4}	-26.2

Table II. Configuration and energy of an isolated vacancy with $r/r_o = 1$ using 6-7 potential. The vacancy is located at (0,0,0) and the relaxations of the neighbors are tabulated.

$E_D^0 = 2035$ cal/mole

(1,	1,	0)	(2,	0,	0)	(2,	1,	1)	ΔE
1.3751×10^{-2}	1.3751×10^{-2}	0	-	-	-	-	-	-	-80.7 cal/mole
1.3770×10^{-2}	1.3770×10^{-2}	0	-5.484×10^{-3}	0	0	-	-	-	-83.8
1.4766×10^{-2}	1.4766×10^{-2}	0	-5.579×10^{-3}	0	0	2.287×10^{-3}	1.410×10^{-3}	1.410×10^{-3}	-87.2

Table III. Energy of substitution and configuration around a krypton impurity in an argon lattice assuming a 6-12 potential. The kyrpton is located at (0,0,0). The relaxations of the neighbors are tabulated

$E_D^0 = -806$ cal/mole

(1,	1,	0)	(2,	0,	0)	(2,	1,	1)	ΔE
-7.985×10^{-3}	-7.985×10^{-3}	0	-	-	-	-	-	-	-57.8 cal/mole
-7.985×10^{-3}	-7.985×10^{-3}	0	1.414×10^{-3}	0	0	-	-	-	-58.2
-8.555×10^{-3}	-8.555×10^{-3}	0	1.414×10^{-3}	0	0	-1.826×10^{-3}	-1.114×10^{-3}	-1.114×10^{-3}	-61.7

Table IV. Energy of substitution and configuration around a neon impurity in an argon lattice assuming a 6-12 potential. The neon is located at (0,0,0). The relaxations of the neighbors are tabulated.

$E_D^0 = 2221$ cal/mole

(1,	1,	0)	(2,	0,	0)	(2,	1,	1)	ΔE
9.051×10^{-3}	9.051×10^{-3}	0	-	-	-	-	-	-	-54.5 cal/mole
9.051×10^{-3}	9.051×10^{-3}	0	-2.312×10^{-3}	0	0	-	-	-	-55.3
9.781×10^{-3}	9.781×10^{-3}	0	-2.375×10^{-3}	0	0	1.899×10^{-3}	1.180×10^{-3}	1.180×10^{-3}	-59.0

Table V. The energy and configuration of a vacancy as a function of r/r_o using a 6-12 potential. The vacancy is located at (0,0,0). The relaxations of the neighbors are tabulated.

r/r_o	(1,	1,	0)	E_D°	ΔE
1.05	-6.603×10^{-3}	-6.603×10^{-3}	0	1903 cal/mole	-11.1 cal/mole
1.03	-1.02×10^{-4}	-1.02×10^{-4}	0	1980	-0
1.02	2.328×10^{-3}	2.328×10^{-3}	0	2009	-2.4
1.01	4.330×10^{-3}	4.330×10^{-3}	0	2028	-10.1
1.00	6.055×10^{-3}	6.055×10^{-3}	0	2035	-23.5
.99	7.514×10^{-3}	7.514×10^{-3}	0	2027	-43.2
.96	1.0844×10^{-2}	1.0844×10^{-2}	0	1878	-148
.94	1.2470×10^{-2}	1.2470×10^{-2}	0	1623	-269
.92	1.3773×10^{-2}	1.3773×10^{-2}	0	1177	-450
.90	1.4836×10^{-2}	1.4836×10^{-2}	0	453	-711
.88	1.5732×10^{-2}	1.5733×10^{-2}	0	-672	-1086

Table VI. The energy and configuration of a vacancy as a function of r/r_o using a 6-7 potential. The vacancy is located at (0,0,0). The relaxations of the neighbors are tabulated.

r/r_o	(1,	1,	0)	E_D°	ΔE
1.06	5.059×10^{-3}	5.059×10^{-3}	0	1921 cal/mole	-5.2 cal/mole
1.04	8.562×10^{-3}	8.562×10^{-3}	0	1979	-19.5
1.02	1.1416×10^{-2}	1.1416×10^{-2}	0	2019	-44.1
1.00	1.3751×10^{-2}	1.3751×10^{-2}	0	2035	-80.7
.98	1.5720×10^{-2}	1.5720×10^{-2}	0	2015	-132
.96	1.7344×10^{-2}	1.7344×10^{-2}	0	1949	-202
.94	1.8719×10^{-2}	1.8719×10^{-2}	0	1820	-295
.92	2.0000×10^{-2}	2.0000×10^{-2}	0	1605	-417
.90	2.1032×10^{-2}	2.1032×10^{-2}	0	1276	-576
.88	2.1989×10^{-2}	2.1989×10^{-2}	0	796	-782
.86	2.2821×10^{-2}	2.2821×10^{-2}	0	117	-1048
.84	2.3547×10^{-2}	2.3547×10^{-2}	0	-827	-1393

Table VII. Configuration and energy of a vacancy with $r/r_o = .9$ and a 6-12 potential. The vacancy is located at (0,0,0). The relaxations of the neighbors are tabulated.

$E_D^0 = 453$ cal/mole

(1,	1,	0)	(2,	0,	0)	(2,	1,	1)	ΔE
1.4836×10^{-2}	1.4836×10^{-2}	0	-	-	-	-	-	-	-711 cal/mole
1.4853×10^{-2}	1.4853×10^{-2}	0	-1.919×10^{-3}	0	0	-	-	-	-714
1.6140×10^{-2}	1.6140×10^{-2}	0	-2.129×10^{-3}	0	0	3.582×10^{-3}	2.157×10^{-3}	2.157×10^{-3}	-775

Table VIII. Configuration and energy of a vacancy with $r/r_o = .9$ and a 6-7 potential. The vacancy is located at (0,0,1). The relaxations of the neighbors are tabulated.

$E_D^0 = 1276$ cal/mole

(1,	1,	0)	(2,	0,	0)	(2,	1,	1)	ΔE
2.1032×10^{-2}	2.1032×10^{-2}	0	-	-	-	-	-	-	-576 cal/mole
2.1070×10^{-2}	2.1070×10^{-2}	0	-3.594×10^{-3}	0	0	-	-	-	-580
2.2875×10^{-2}	2.2875×10^{-2}	0	-4.008×10^{-3}	0	0	4.899×10^{-3}	2.953×10^{-3}	2.953×10^{-3}	-613

At first, the relaxations appear to be intuitively incorrect. However, an examination of the geometry of the lattice shows that for each relaxation, the motion of the atoms always increases the overlap with some atoms and decreases the overlap with others. The inward relaxation of the nearest neighbors is obvious, and the small magnitude of the relaxation can be accounted for on the basis of the fact that some of the nearest neighbors of the vacancy are also nearest neighbors of the relaxing atom. For example, the atom at (1,1,0) has as its nearest neighbors atoms at (1,0,1), (1,0,-1), (0,1,1), and (0,1,-1). The inward motion of these atoms increases the overlap between the atom (1,1,0) and the four mentioned atoms relaxing inwards that are its nearest neighbors as well as the nearest neighbors of the vacancy. At the same time the overlap with the vacancy disappears, and the overlap with the remaining seven nearest neighbors is decreased. Thus the total relaxation and its direction are the result of both increasing and decreasing overlaps.

Again for second nearest neighbors any movement in the lattice increases overlap, serving to keep the relaxation small. However, here the interaction between two of the relaxing (next-nearest neighbor) atoms is small and the most important term is the absence of the attraction of the center atom, thus leading to a relaxation outward. The behavior of the third nearest neighbors cannot be accounted for in this way. The largest term seen by a third nearest neighbor is not the absence of the attraction of the central atom, which is already a very small term. Rather the important terms are due to the motion of its own nearest neighbors (two of which are nearest neighbors to the defect and one a next-nearest neighbor). It is into the potential hole created by

the movement of these nearest neighbors that the third nearest atom moves. As pressure on the lattice is increased (interatomic distance is decreased), nearest neighbors of the vacancy are farther up on the repulsive side of the central atom and so can relax further into the hole. Next nearest neighbors are less strongly attracted to the central atom and so move less away from the central atom. At sufficiently high pressure they would actually move toward the defect. The increased movement of the first two layers toward the vacancy leaves the third nearest neighbors a larger hole in which to relax, and so their motion toward the center increases with pressure. That the relaxation of the third nearest neighbors contributes more to ΔE than the second nearest neighbor is understandable as there are twenty-four next-next-nearest neighbors and only six next-nearest neighbors.

Expectedly, the relaxations of the atoms around a krypton (large) impurity (Table III), are of the opposite sign from those around a vacancy, and a neon (small) impurity (Table IV) affects the lattice qualitatively like a vacancy, except that the attraction of the neon increases the relaxations.

For relaxations around an internal defect ΔE is found to converge less rapidly than for surface relaxations.[12] Also the numerical values of the relaxations for internal effects are of less significance than those for surfaces, as these calculations are highly dependent on the repulsive potential, which is not accurate, while the latter depend mostly on the $1/r^6$ attractive potential, whose form is well established.

Correcting the energy of formation of a vacancy at zero pressure determined for three layers of relaxation, we find the following:

6-12 Potential

$E_V^\circ = 2035$ cal/mole

$E_V = 2014$ cal/mole

$\frac{\Delta E}{E_V^\circ} = -1.3 \times 10^{-2}$

6-7 Potential

$E_V^\circ = 2035$ cal/mole

$E_V = 1948$ cal/mole

$\frac{\Delta E}{E_V^\circ} = -4.4 \times 10^{-2}$

By varying the interatomic distance used in the calculations it is possible to consider formation of vacancies under high pressure or at a hypothetical distended or compressed lattice. This was done for interatomic distances ranging from 1.06 to .84 times the normal distance; the results of these calculations are shown in Tables V-VIII.

As expected the relaxations inward increased with decreasing separation. For a 6-12 potential the sign of the first relaxation changes at about 1.03 the normal distance so that nearest neighbors relax away from the vacancy. The volume at this distance corresponds roughly to the volume in liquid argon. Whether this correspondence is coincidental or of some significance has not been studied as the behavior of the lattice under high pressure was of greater interest to us.

At sufficiently small separations, even before the energy of vaporization becomes positive, the potential energy of formation of a vacancy becomes negative. There are two processes which may be ex-

amined in the formation of a vacancy: a constant volume process, in which case ΔA is the important thermodynamic function, and a constant pressure process for which ΔF is of interest.

For constant pressure creation of a vacancy we consider an interior atom removed to the surface of the crystal.

$$\Delta F = \Delta E + P\Delta V - T\Delta S$$

where ΔE now refers to the energy of formation of a vacancy with relaxations, $T = 0$, and P is obtained from the potential from

$$P = \left(- \frac{\partial E_S}{\partial V} \right)_T = - \left(\frac{\partial E_S}{\partial r} \right)_T \left(\frac{1}{\partial V / \partial r} \right)_T$$

noting that E_S is the average energy of sublimation. For $r = .9$ we obtained

6-12 Potential

$\Delta F = 13181$ cal/mole

6-7 Potential

$\Delta F = 6605$ cal/mole

The constant volume process, for the formation of one vacancy per n atoms, may be regarded in the following way: Starting with n atoms with separation r, we go to n atoms and a vacancy in a lattice with interatomic distance $r' = \left(\frac{n}{n+1} \right)^{1/3} r$. For this process we may readily compute ΔA and obtain the following values for the formation of one vacancy per n atoms, with $r = .9$:

6-12 Potential

n	ΔA (cal/mole)
100	13400
1,000	13219
10,000	13185

6-7 Potential

n	ΔA (cal/mole)
100	6676
1,000	6615
10,000	6612

Comparing the computed values of ΔF and ΔA with the average energy of sublimation at zero pressure (2035 cal/mole), we would expect that at some not too high temperature the lattice would disorder, whatever the actual form of the potential is. This is in agreement with the shock work of Alder et al.[16] who found a first order transition in solid argon lying on the extension of the normal melting curve.

3. Di-Defects

a. Method. In this section we assume (1) that there are two neighboring vacancies located at (0,0,0) and (1,1,0), (2) that only nearest neighbors to the di-defect relax, and (3) that the relaxations retain the symmetry of the lattice. On this basis it becomes possible to write an expression for the relaxation energy similar to that of an isolated vacancy. This expression can be readily modified to calculate relaxation energies for a vacancy next to an impurity atom or, as with the isolated vacancy, for divacancy formation in a compressed lattice.

Next to such a di-defect there are eighteen nearest neighbors plus the impurity atom in that case. Considering the symmetry of the lattice the problem becomes one of minimizing an energy function in sixteen variables. This was done on an IBM 7094 using the same technique employed with the isolated defect. Fortunately, it was found that the modified half interval technique used did lead to a convergent solution.

b. Results. The di-defect results are given in Tables IX and X. The energy required to produce a given defect in a perfect lattice without relaxation is E_D°, the relaxation energy is ΔE, and the energy required to produce the defect is E_D. Obviously

$$E_D = E_D^\circ + \Delta E$$

The energy required to introduce a vacancy next to the other part of the defect (vacancy or impurity) in a relaxed lattice, E_V, is the quantity of real interest in these calculations. This value is also given in Table IX.

The relaxations themselves are presented in Table X. In all cases the relaxations themselves are small, being of the same order of magnitude as for isolated defects. It was found that a krypton atom relaxes 1.5% into the vacancy and a neon atom relaxes 3.6%. These relaxations are small as for the pure material; the impurity atom rapidly increases its overlap with its other nearest neighbors. Relaxations into the di-vacancy behaved like those into the isolated vacancy. All nearest neighbors relaxed inwards towards the vacancy-vacancy and the neon-vacancy defects. In the case of a krypton-vacancy defect, the neighboring atoms moved towards the vacancy and away from the krypton impurity as expected from the isolated defect calculations.

Table IX. The energy of formation of a di-defect. E_D° is the energy with relaxation. ΔE the relaxation energy, E_D is $E_D^\circ + \Delta E$, and E_V is the energy required to form a vacancy adjacent to the other part of the defect.

Defect	E_D°	ΔE	E_D	E_V
Vac-Vac $r/r_o = 1$ 6-12 Potential	3955 cal/mole	-57.5 cal/mole	3987 cal/mole	1888 cal/mole
Vac-Vac $r/r_o = .90$ 6-12 Potential	970	-1913	-943	-621
Vac-Kr	989	-78.8	910	1778
Vac-Ne	4141	-102.2	40.39	1877

Table X.

The vacancy is at (0,0,0) and the second defect at (1,1,0). The point (x,y,z) (given as $\begin{pmatrix} x \\ y \\ z \end{pmatrix}$ in the Table) goes to (x-δx, y-δy, z-δz). $\begin{pmatrix} \delta x \\ \delta y \\ \delta z \end{pmatrix}$ is given for each second defect and point investigated. For comparison, relaxations around a single vacancy in a perfect lattice are given under Ar for those points considered in di-defect studies.

	Di-defect Relaxations			
$\begin{pmatrix} x \\ y \\ z \end{pmatrix}$	Vac.	Ne	Ar	Kr
$\begin{pmatrix} 1 \\ 1 \\ 0 \end{pmatrix}$	0 0 0	-3.5937×10^{-2} -3.5937×10^{-2} 0	6.420×10^{-3} 6.420×10^{-3} 0	1.7026×10^{-2} 1.7026×10^{-2} 0
$\begin{pmatrix} 1 \\ 0 \\ 1 \end{pmatrix}$	7.880×10^{-3} -7.851×10^{-3} 2.113×10^{-2}	8.242×10^{-3} -1.1821×10^{-2} 2.6435×10^{-2}	6.420×10^{-3} 0 6.420×10^{-3}	4.194×10^{-3} 1.0234×10^{-2} -7.685×10^{-3}
$\begin{pmatrix} 1 \\ 0 \\ -1 \end{pmatrix}$	7.880×10^{-3} -7.851×10^{-3} -2.1113×10^{-2}	8.242×10^{-3} -1.1821×10^{-2} -2.6435×10^{-2}	6.420×10^{-3} 0 -6.420×10^{-3}	4.194×10^{-3} 1.0234×10^{-2} 7.685×10^{-3}
$\begin{pmatrix} 0 \\ 1 \\ 1 \end{pmatrix}$	-7.851×10^{-3} 7.880×10^{-3} 2.1113×10^{-2}	-1.1821×10^{-2} 8.242×10^{-3} 2.6435×10^{-2}	0 6.420×10^{-3} 6.420×10^{-3}	1.0234×10^{-2} 4.194×10^{-3} -7.685×10^{-3}
$\begin{pmatrix} 0 \\ 1 \\ -1 \end{pmatrix}$	-7.851×10^{-3} 7.880×10^{-3} -2.1113×10^{-3}	-1.1821×10^{-2} 8.242×10^{-3} -2.6435×10^{-2}	0 6.420×10^{-3} -6.420×10^{-3}	1.0234×10^{-2} 4.194×10^{-3} 7.685×10^{-3}
$\begin{pmatrix} -1 \\ 0 \\ 1 \end{pmatrix}$	-6.333×10^{-3} -8.00×10^{-4} 5.922×10^{-3}	-7.216×10^{-3} -1.552×10^{-3} 6.240×10^{-3}	-6.420×10^{-3} 0 6.420×10^{-3}	-4.980×10^{-3} 1.230×10^{-3} 6.240×10^{-3}

Table X. (Continued)

	Di-Defect Relaxations			
$\begin{pmatrix} x \\ y \\ z \end{pmatrix}$	Vac.	Ne	Ar	Kr
$\begin{pmatrix} -1 \\ 0 \\ -1 \end{pmatrix}$	-6.333×10^{-3} -8.00×10^{-4} -5.922×10^{-3}	-7.216×10^{-3} -1.552×10^{-3} -6.240×10^{-3}	-6.420×10^{-3} 0 -6.420×10^{-3}	-4.980×10^{-3} 1.230×10^{-3} -6.240×10^{-3}
$\begin{pmatrix} 0 \\ -1 \\ 1 \end{pmatrix}$	-8.00×10^{-4} -6.333×10^{-3} 5.922×10^{-3}	-1.552×10^{-3} -7.216×10^{-3} 6.240×10^{-3}	0 -6.420×10^{-3} 6.420×10^{-3}	1.230×10^{-3} -4.980×10^{-3} 6.240×10^{-3}
$\begin{pmatrix} 0 \\ -1 \\ -1 \end{pmatrix}$	-8.00×10^{-4} -6.333×10^{-3} -5.922×10^{-3}	-1.552×10^{-3} -7.216×10^{-3} -6.240×10^{-3}	0 -6.420×10^{-3} -6.420×10^{-3}	1.230×10^{-3} -4.980×10^{-3} -6.240×10^{-3}
$\begin{pmatrix} 1 \\ -1 \\ 0 \end{pmatrix}$	4.121×10^{-3} 1.31×10^{-4} 0	3.603×10^{-3} -5.95×10^{-4} 0	6.420×10^{-3} -6.420×10^{-3} 0	6.513×10^{-3} -9.750×10^{-3} 0
$\begin{pmatrix} -1 \\ 1 \\ 0 \end{pmatrix}$	1.31×10^{-4} 4.121×10^{-3} 0	-5.95×10^{-4} 3.603×10^{-3} 0	-6.420×10^{-3} 6.420×10^{-3} 0	-9.750×10^{-3} 6.513×10^{-3} 0
$\begin{pmatrix} -1 \\ -1 \\ 0 \end{pmatrix}$	-6.079×10^{-3} -6.079×10^{-3} 0	-6.328×10^{-3} -6.328×10^{-3} 0	-6.420×10^{-3} -6.420×10^{-3} 0	-5.566×10^{-3} -5.566×10^{-3} 0
$\begin{pmatrix} 2 \\ 2 \\ 0 \end{pmatrix}$	6.079×10^{-3} 6.079×10^{-3} 0	7.343×10^{-3} 7.343×10^{-3} 0	* * *	-2.900×10^{-3} -2.900×10^{-3} 0

Comparison of E_V in Table IX with the energy required to produce an isolated vacancy indicates that the energy of formation of a vacancy next to another defect is lower than that for an isolated vacancy. Free energies for formation of vacancies are correspondingly lower. This is in agreement with the attraction of vacancies predicted by Stripp et al.[31]

It is possible from these results to estimate the relative concentrations of various defects. Following Kröger and Vink,[33] we write the concentration of a given defect [D] as

$$[D] = e^{S_D/k} e^{-E_D/kT}$$

where S_D is the entropy of formation of the defect and E_D is the total energy required to produce the defect. S_D may be calculated from elementary statistics. E_D may be separated into a kinetic energy term, K_D, and a potential energy term, E_D. This latter term has been obtained in this paper for various modes of vacancy formation. If we assume that, in the formation of a vacancy, K_V is independent of the location of the vacancy, we obtain

$$\frac{[V]}{[V_o]} = \frac{e^{S_V/k} e^{-E_V/kT}}{e^{S_{V_o}/k} e^{-E_{V_o}/kT}}$$

for the relative concentrations of two types of (vacancy) defects. $\frac{[V]}{[V_o]}$ is plotted in Figs. 1 and 2 for various types of vacancies, where $[V_o]$ is always the concentration of isolated vacancies in a pure argon lattice. $[V_o]$ has been estimated by Foreman and Lidiard to be .1% near the melting point of argon. From a knowledge of the concentration of isolated vacancies in pure argon, we can obtain the concentration of various types of di-defects.

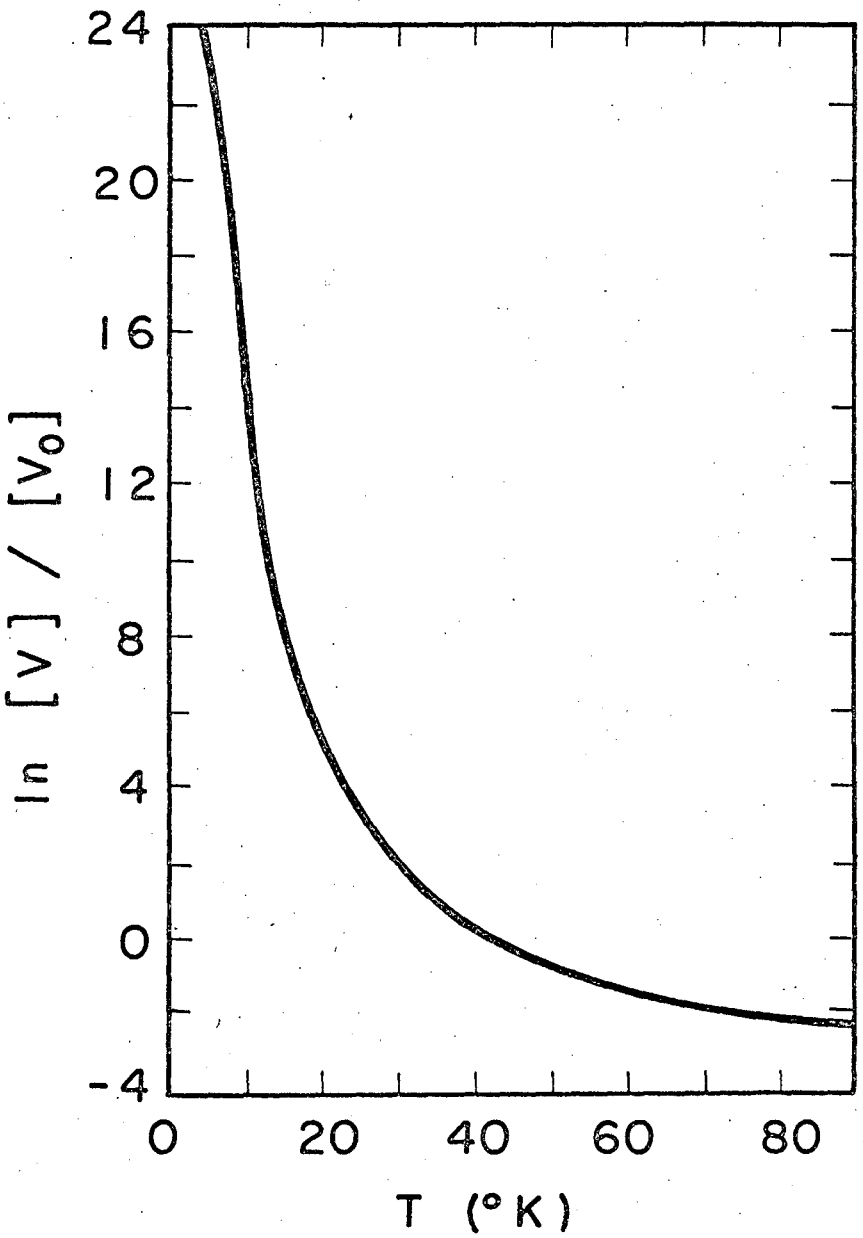

MUB-8155

Fig. 1 $\ln \frac{[V]}{[V_o]}$ where $[V_o]$ is concentration of isolated vacancies in pure Ar and [V] is the concentration of vacancies adjacent to Kr atoms in argon with .1% Kr.

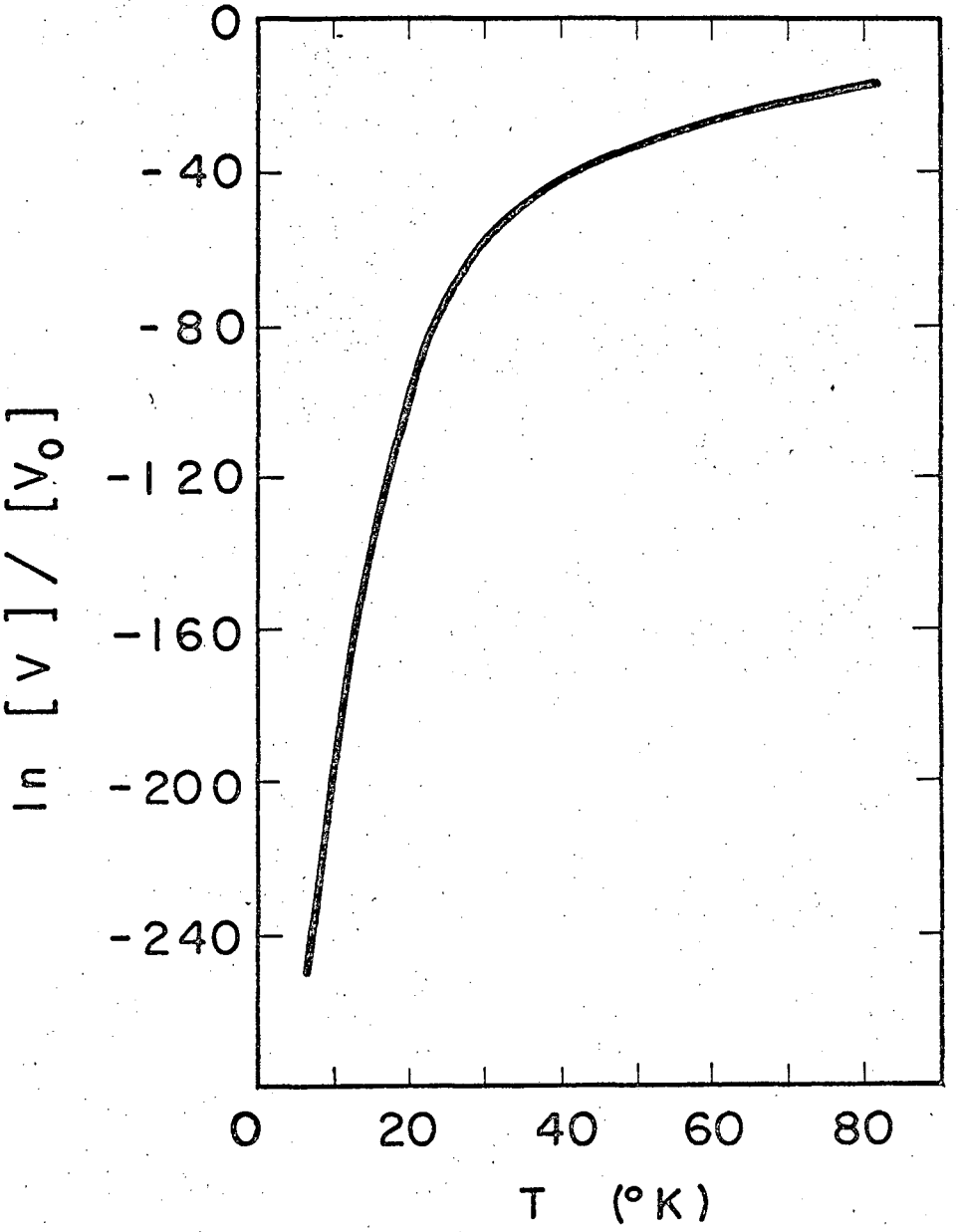

MUB-8154

Fig. 2 $\ln \frac{[V]}{[V_o]}$ where $[V_o]$ is concentration of isolated vacancies in pure Ar and [V] of divacancies in pure Ar.

From Fig. 1 we see that the formation of a vacancy next to a krypton atom is strongly preferred at low temperatures and less so at higher temperatures. Concentration of vacancies next to neon impurities behaves similarly. Concentration of di-vacancies is insignificant in comparison with the concentration of vacancies except at high temperatures (> 80°K) where we approach the melting point of argon; this is shown in Fig. 2.

The preference for formation of a vacancy next to an impurity causes a decrease in the average energy of formation of a vacancy in impure argon, particularly at low temperatures; average energy of vacancy formation is plotted in Fig. 3 as a function of krypton concentration at various temperatures. The values shown here for high impurity concentration are almost certainly not valid since the impurities will interact, and this interaction has not been included in the calculations. Similar curves are obtained for neon.

The energy average required to produce a vacancy in an impure lattice may be obtained from Fig. 3. This we have used to estimate the concentration of vacancies in an impure argon lattice at 80°K, which is shown in Fig. 4. Impurities are seen to increase the concentration of vacancies. Again values for large impurity concentrations are not significant. Even in impure samples the concentration of vacancies predicted by this model is much smaller than that determined experimentally.

4. Conclusions

The qualitative behavior of the relaxations around a vacancy are fairly independent of the exact form of the repulsive potential. As one would intuitively expect, the effect of high pressure is to drive surrounding atoms further into the hole left by a vacancy. For atoms more distant from a defect than second nearest neighbors, the most important

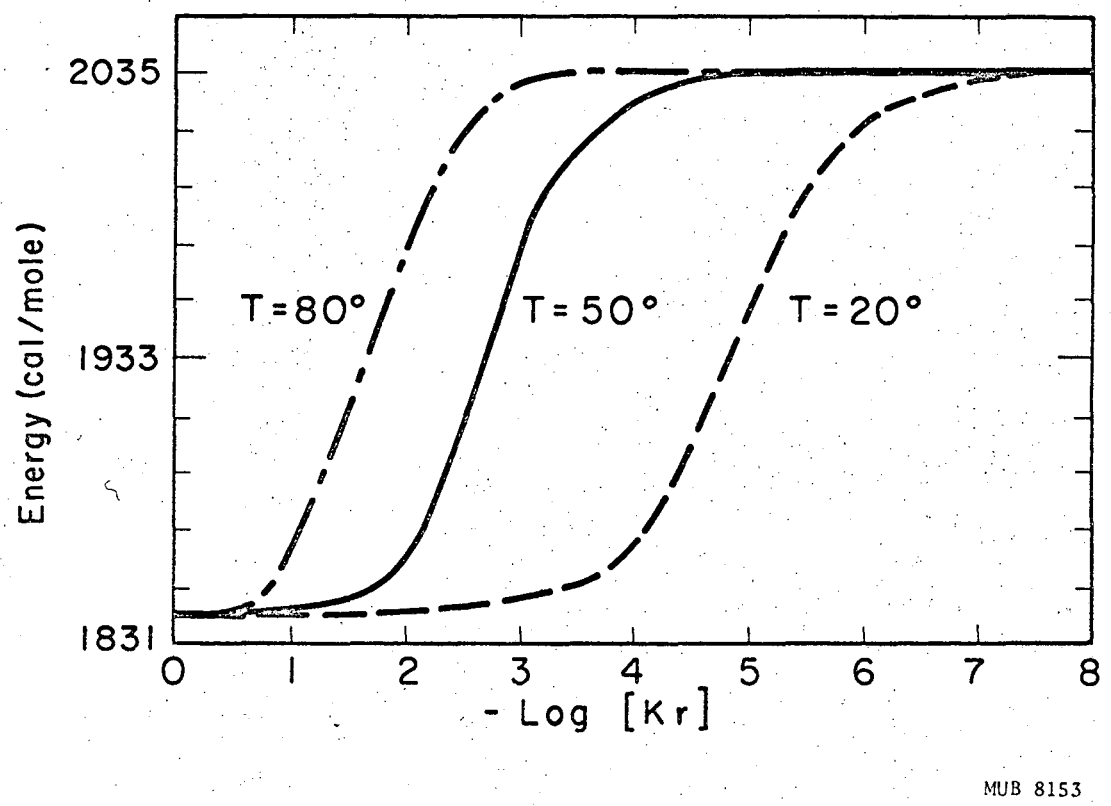

Fig. 3 Average energy of creation of a vacancy in an impure lattice vs -log (krypton concentration).

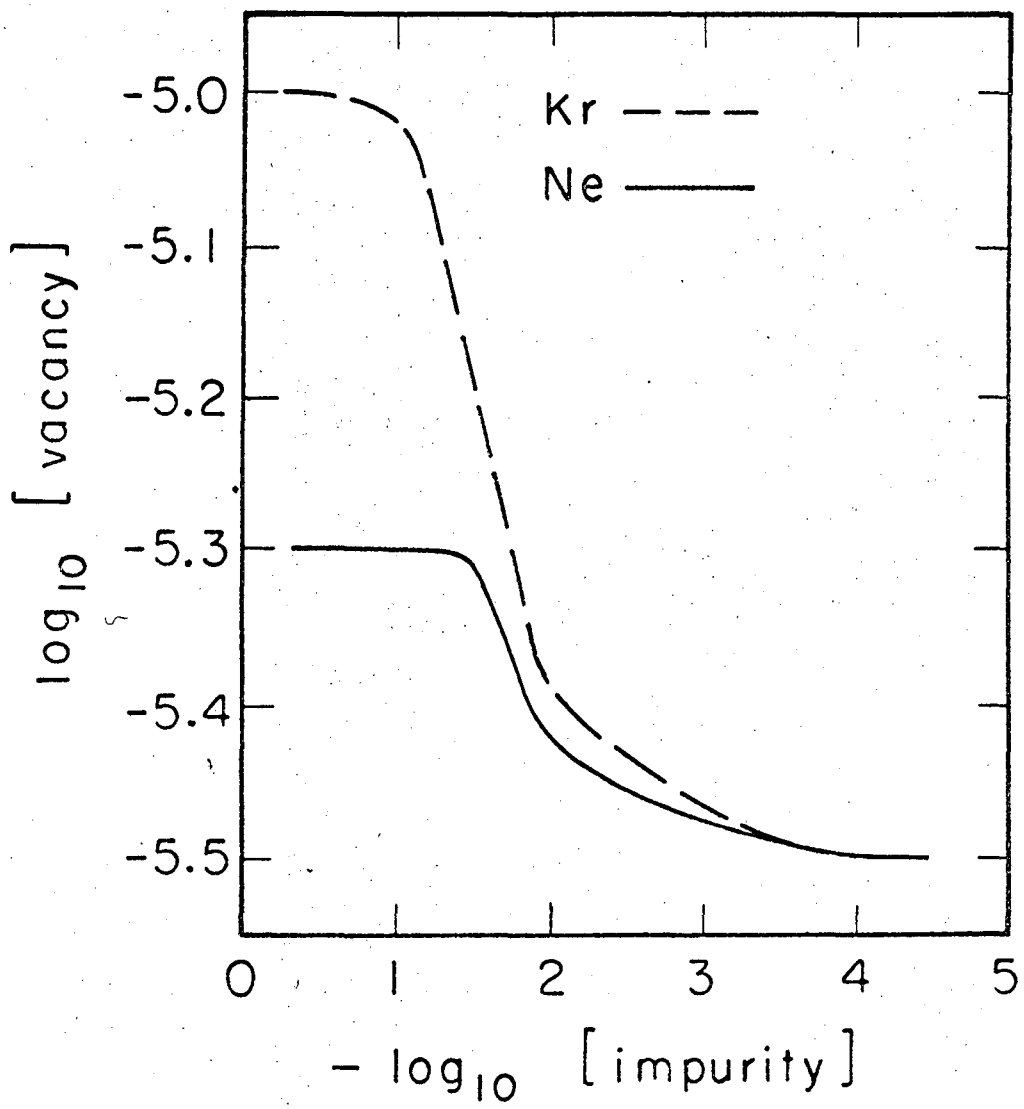

MUB-8288

Fig. 4 log [vacancy] vs -log [impurity] at 80°K

contribution to their motion is the behavior of their own nearest neighbors.

Relaxations around small atoms are qualitatively like those around vacancies, while relaxations around large atoms are opposite in sign to those around vacancies.

At high pressure it was found that an order-disorder transition could occur at not too high temperature.

It was found that formation of a vacancy next to another defect is energetically preferred to formation of an isolated vacancy. We have shown that the concentration of vacancies next to impurity atoms is higher than that which would be expected from a random distribution of vacancies, particularly at low temperatures. From this we conclude that the concentration of vacancies at a given temperature increases with impurity concentration.

We have also shown that the concentration of di-vacancies is insignificant in pure argon except at high temperatures ($> 80°K$) where we approach the melting point of pure argon.

D. Diffusion in Solids

1. Introduction

Theoretical calculations of self-diffusion coefficient have been made for copper[34-36] and argon.[37] Even though the calculations for copper present a number of serious problems, rough agreement with experiment has been obtained. It would appear that more precise calculations could be made for argon than for copper since argon, for computational purposes, is reasonably well represented by a two-body potential and does not have the complications of free electrons or core polarization. Fieschi et al.[37] have done extensive calculations on the self-diffusion coefficient in solid argon and have obtained results that are partially in agreement with experiments.[38] Their exponential term is roughly 25% lower and the pre-exponential term differs by 10^4 from the experimental values.

Fieschi and coworkers estimated the barrier to diffusion by allowing the four nearest neighbors of the diffusing atoms to relax while the atom and vacancy interchanged. In Sec. I-C, a program was developed which permits the calculation of the energy when all of the nearest neighbors of an adjacent pair of lattice sites are perturbed either by the substitution of an impurity or a vacancy, or by a combination of the two.

The expanded treatment of self-diffusion in this section gives a closer agreement with the observed activation energy than that of the earlier computation. Furthermore, the work done suggests that diffusion may occur equally well by the exchange of an atom with a divacancy rather than a monovacancy. It is true that the number of divacancies is low compared to the number of monovacancies, but the barrier is approximately the same, and this mechanism leads to a higher pre-exponential term when

the Arrhenium equation is used to describe the diffusion process.

It is evident that these and similar computations are really only approximations, and the numerical values obtained are highly limited by the assumptions that are necessary at the present time. However, it is felt that sufficient insight into the physical process can be obtained to warrant the effort that is expended.

2. Theory

It is known that most experimental diffusion coefficients[39] can be fit by the Arrhenius equation

$$D = D_o \, e^{-E/RT} \qquad (1)$$

where D_o, the "frequency factor" and E, the "activation energy" are constants. In some cases D_o and E have been found to be temperature dependent.[40,41]

For diffusion via some lattice defect the Arrhenius equation (Eq. 1) may be expressed as[39,42]

$$D = \gamma a^2 \nu \, e^{S_D^\dagger/R} \, e^{S_D/R} \, e^{-E_D^\dagger/RT} \, e^{-E_D/RT} \qquad (2)$$

γ is a numerical factor roughly equal to unity, a is the length of one diffusion jump (a is equal to the solid interatomic distance for most vacancy diffusion mechanisms), ν is the vibrational frequency of the diffusing atom, S_D and E_D are the entropy and energy of formation of the lattice defects, and $S_D^\dagger$ and $E_D^\dagger$ are the activation entropy and energy of the motion. $E_D^\dagger$ is the difference in energy between states 1 and 2 in Fig. 5, the usual reaction coordinate diagram.

Diffusion is assumed to occur by interchange of an atom with a vacancy at a nearest neighbor site (Fig. 6). We assume that as the

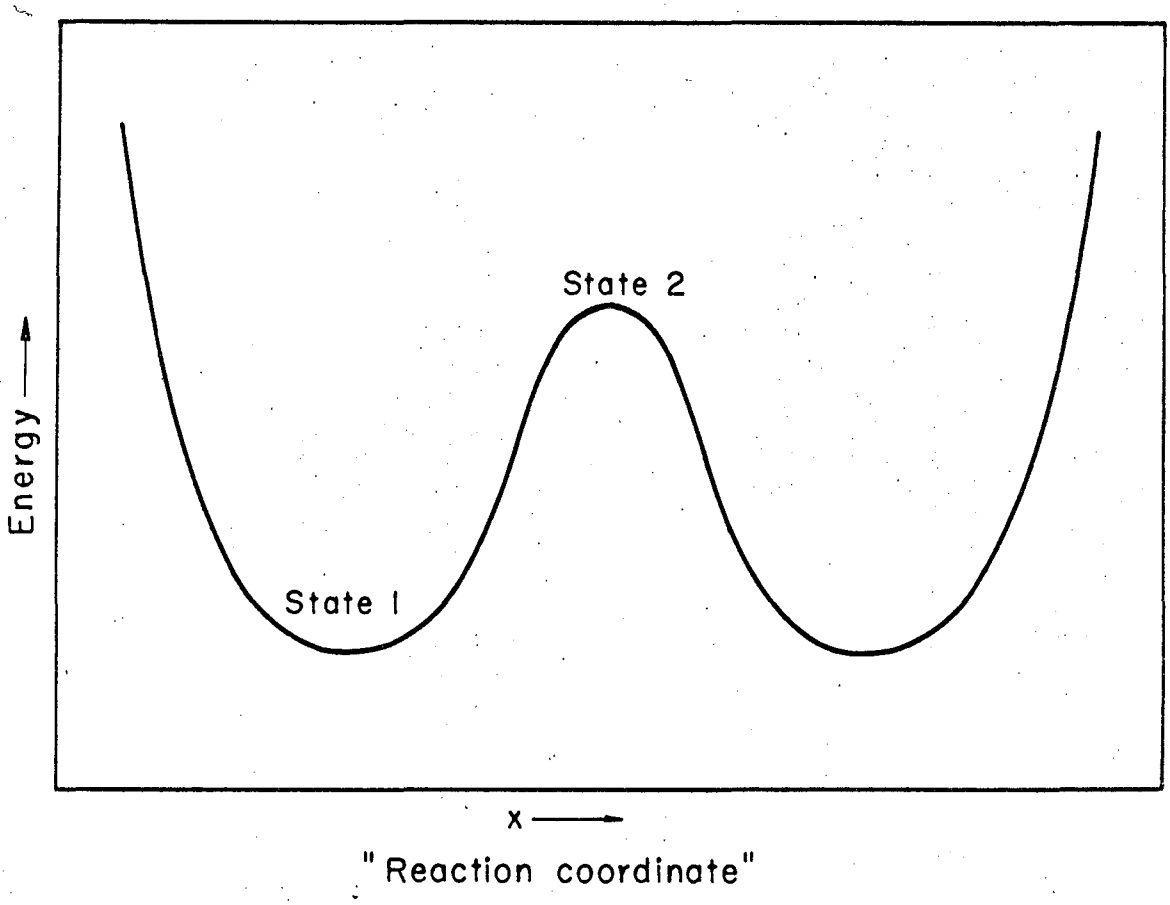

MUB 11560

Fig. 5 The reaction coordinate diagram for diffusion.

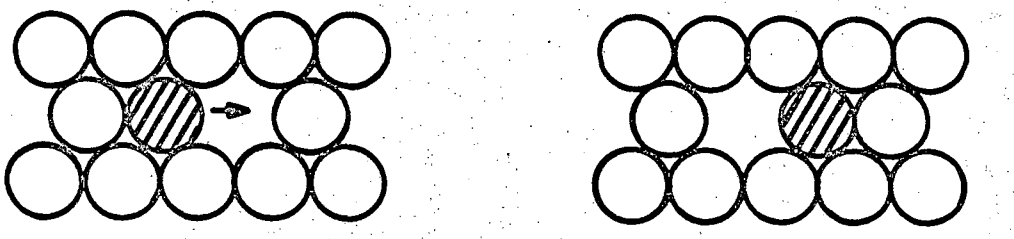

Fig. 6 Exchange with a monovacancy; diffusing atom is cross hatched.

diffusing atom moves, the lattice continuously relaxes to a minimum potential configuration. In this way, we consider correlation of the diffusing atom with its neighbors to obtain a potential energy diagram for use in an equilibrium calculation. We also assume that $E_D^{\dagger}$ in Eq. (2) is the difference in the potential energies of states 1 and 2 in Fig. 5, where state 1 represents now the minimum potential configuration of the lattice with a vacancy and state 2 the minimum potential configuration of the lattice with the diffusing atom displaced half the distance between its lattice site and that of the vacancy.

3. Calculations

Using techniques developed in Sec. I-C, it is possible to compute the potential energy, $E_o(x)$, required to move the diffusing atom from its normal lattice site to a distance x along the "reaction coordinate", Fig. 7, in an undeformed lattice.

The eighteen nearest neighbors to the di-defect (diffusing atom plus vacancy) were allowed to relax to the configuration of minimum potential energy; the difference in potential energy between the unrelaxed lattice and the minimum potential configuration with the diffusing atom at x is designated $\Delta E(x)$. Allowing only nearest neighbors to relax and considering the symmetry of the lattice, determination of $\Delta E(x)$ is reduced to simultaneously minimizing an expression in sixteen independent variables. This minimization was carried out by an iterative half interval technique which fortunately converged. The relaxations of the nearest neighbors were found to be small throughout the diffusion process and are presented in Table XI for states 1 and 2 for self-diffusion. Because of the great amount of machine time required to extend consideration to relaxations of more distant neighbors and the only qualitative

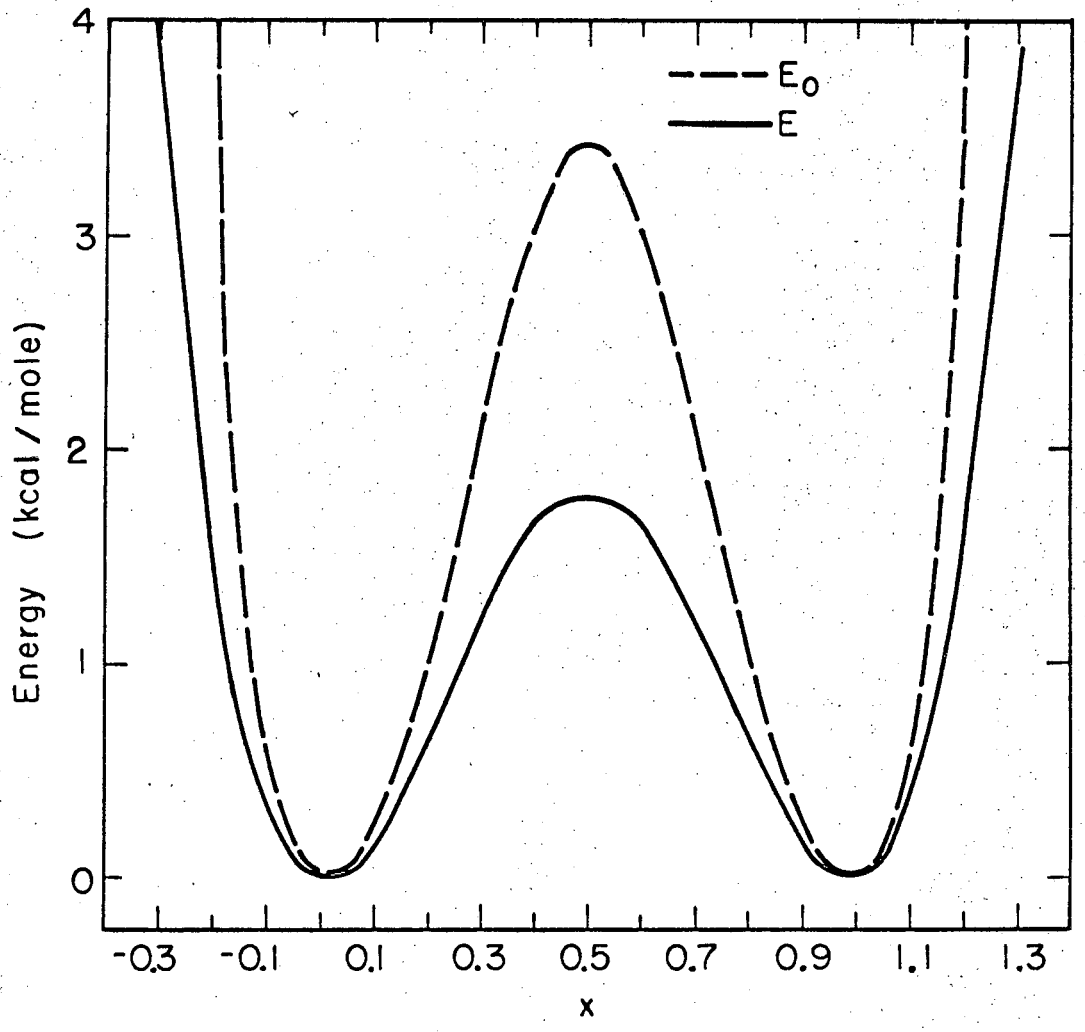

MUB-11559

Fig. 7 Energy as a function of position for diffusion via monovacancy exchange; E_o is without relaxations, E is with relaxations.

Table XI

Relaxations of the nearest neighbors for mono-vacancy self diffusion. The moving atom is initially at (1,1,0) and the vacancy at (0,0,0). The relaxing atoms are grouped into sets of points equivalent by symmetry:

(1,1,0)

(1,0,1) ≡ (1,0,-1) ≡ (0,1,1) ≡ (0,1,-1)

(-1,0,1) ≡ (-1,0,-1) ≡ (0,-1,1) ≡ (0,-1,-1)

(1,-1,0) ≡ (-1,1,0)

(-1,-1,0)

(2,2,0)

(1,2,1) ≡ (1,2,-1) ≡ (2,1,1) ≡ (2,1,-1)

(2,0,0) ≡ (0,2,0)

$\begin{pmatrix}\delta x\\ \delta y\\ dz\end{pmatrix}$ is given for States 1 and 2 (Fig. 5) for one atom of each set

x y z	State 1	State 2
$\begin{pmatrix}1\\1\\0\end{pmatrix}$	6.42×10^{-3} 6.42×10^{-3} 0	.5 .5 0
$\begin{pmatrix}1\\0\\1\end{pmatrix}$	6.42×10^{-3} 0 6.42×10^{-3}	-2.58×10^{-2} 2.52×10^{-2} -6.88×10^{-2}
$\begin{pmatrix}-1\\0\\1\end{pmatrix}$	6.42×10^{-3} 0 6.42×10^{-3}	-1.17×10^{-2} -1.88×10^{-3} 9.06×10^{-3}
$\begin{pmatrix}1\\-1\\0\end{pmatrix}$	6.42×10^{-3} -6.42×10^{-3} 0	1.37×10^{-2} -2.63×10^{-2} 0
$\begin{pmatrix}-1\\-1\\0\end{pmatrix}$	-6.42×10^{-3} -6.42×10^{-3} 0	-6.25×10^{-3} -6.25×10^{-3} 0

Table XI (Continued)

x y z	State 1	State 2
$\begin{pmatrix}2\\2\\0\end{pmatrix}$	-2.27×10^{-4} -2.27×10^{-4} 0	6.25×10^{-3} 6.25×10^{-3} 0
$\begin{pmatrix}1\\2\\1\end{pmatrix}$	5.39×10^{-4} 8.80×10^{-4} 5.39×10^{-4}	2.50×10^{-4} 1.12×10^{-2} 9.69×10^{-3}
$\begin{pmatrix}2\\0\\0\end{pmatrix}$	-3.43×10^{-3} 0 0	2.69×10^{-2} -1.46×10^{-2} 0

significance of the results, no attempt was made to relax the more distant neighbors. Thus

$$E(x) = E_o(x) - \Delta E(x)$$

is the potential energy required to move the diffusing atom from its relaxed lattice site to the position (x) in the relaxed lattice. E(x) and $E_o(x)$ are shown in Fig. 7. In Fig. 7 the distance between the initial and final lattice positions is one unit. In accordance with our assumptions, we take

$$E_V^\dagger = E(.5)$$

where $E_V^\dagger$ is the energy at the saddlepoint.

Calculations for impurity diffusion are essentially the same as for argon self-diffusion and were made for neon and krypton impurities. The potential of argon was modified as in Sec. I-C.

4. Results

We have developed a method for calculating the potential energy change of the system in going from initial state 1 to intermediate state 2 (Fig. 5); this is E(.5) and is equal to $E_V^\dagger$ in Eq. (2). For self diffusion in argon

$$E_V^\dagger = E(.5) = 1798 \text{ cal}$$

where the units are cal/mole of diffusing atoms. We have obtained in Sec. I-C the energy required to remove an atom from the bulk of argon, leaving an isolated vacancy; the process of physical importance involves the removal of a bulk atom to the surface of the crystal. Assuming that the average binding energy to the surface is half the binding energy to the bulk, we obtained

$$E_V = 2014 \text{ cal}$$

In the Arrhenius Eq. (1)

$$E = E_V^{\dagger} + E_V = 3812 \text{ cal}$$

which is in surprisingly good agreement with the experimental results of Boato[38]

$$D = 15 \times e^{-4120 \text{ cal}/RT} \text{ cm}^2/\text{sec}$$

It is interesting to note that $E_V^{\dagger}$ is only slightly less than one half of E for argon. Comparisons of Mukherjee's[42] tables of E_V for a number of metals with the "activation energies" for diffusion tabulated by Lazarus[39] indicates that this is generally true, assuming the diffusion mechanism is monovacancy exchange.

We have observed above that $E_V^{\dagger}$ and E_V are roughly equal for monovacancy exchange. We have shown in Sec. I-C that the energy of formation of a divacancy, E_{V_2}, is less than twice the energy of formation of a monovacancy, E_V,

$$E_{V_2} = 3897 \text{ cal}$$
$$< 2E_V = 4028 \text{ cal}$$

An atom which is a nearest neighbor to both sites of the divacancy may move by exchanging position with one of the vacancies. This mechanism may be represented in a (111) plane (Fig. 8) and results in a rotation of the divacancy. For this mechanism

$$E_{V_2}^{\dagger} = 1280 \text{ cal}$$

without relaxation; allowing the four atoms nearest to the saddle point to relax reduces $E_{V_2}^{\dagger}$ to

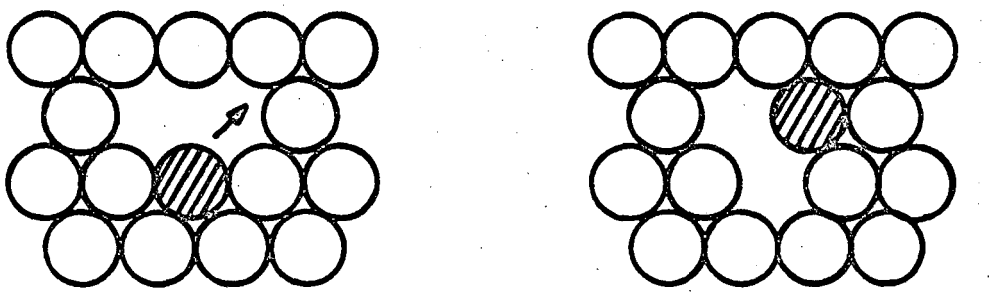

Fig. 8 Rotation of a divacancy; diffusing atom is cross hatched.

$$E^{\dagger}_{V_2} = 950 \text{ cal}$$

No attempt was made to consider additional relaxations. This value of $E^{\dagger}_{V_2}$ is an upper limit and would presumably be reduced by consideration of more relaxations. For divacancy diffusion, the "activation energy" in the Arrhenius expression (Eq. 1) is

$$E = E_{V_2} + E^{\dagger}_{V_2} = 4847 \text{ cal}$$

which is also in reasonable agreement with Boato's experimental result.[38] Diffusion may occur with a divacancy via two other mechanisms. In these the diffusing atom is a nearest neighbor with only one of the sites of the divacancy and exchanges with this site. This results in a splitting of the divacancy leaving two vacancies which are either second or third nearest neighbors depending on which neighbor of the vacancy moves. Both splitting processes have higher barriers than the rotation of the divacancy.

No calculations of $S^{\dagger}_{V_2}$ or S_{V_2} have been made to the author's knowledge. However, S_{V_2} must be larger than S_V and $S^{\dagger}$ is certainly greater for divacancy exchange than for monovacancy.

It would thus appear that, in argon, the "frequency factor" for diffusion via divacancy exchange is greater than that for monovacancy exchange and the "activation energies" for both processes are essentially the same and in reasonable agreement with experiment.[38] This would imply that, in fact, the preferred self-diffusion mechanism in solid argon, and perhaps in other close packed solids, is not monovacancy exchange as has been previously assumed, but rather is divacancy exchange. This conclusion is contrary to intuition, which would indicate that the

concentration of divacancies is too low to be significant. However, though the concentration of divacancies is very low, the barrier for motion is much lower for divacancy exchange than for monovacancy exchange and the "frequency factor" is higher, which may lead, surprisingly, to a higher self-diffusion rate for divacancy exchange.

In order to account for Boato's[38] experimental results, the entropy term for divacancy diffusion must be larger than that calculated by Fieschi[37] for monovacancy diffusion by roughly 10 entropy units. It would be desirable to do extensive calculations on the divacancy exchange mechanism to find whether this very large entropy term is in fact found.

Without difficulty it was possible to compute the "activation energy" in the Arrhenius expression for both examined mechanisms in a compressed argon lattice. Under compression, a $P\Delta V$ term must be included in the "activation energy". We have assumed in Sec. I-C that the formation of a vacancy involves the removal of an atom from the bulk to the surface, that the "volume" of an atom on the perfect surface is equal to the average bulk "volume", and that the surface binding energy is half the bulk binding energy. With these assumptions we obtained the "activation energies" for both processes in the compressed solid; these are shown in Fig. 9 as a function of pressure. Though the "activation" energy for divacancy diffusion at low pressure is comparable to that of monovacancy exchange, at high pressures the divacancy mechanism appears to have a higher "activation energy".

In diffusion work one often studies the so-called "activation volume". Writing

$$\Delta F = \Delta E + P\Delta V - T\Delta S$$

$$\left(\frac{\delta \Delta F}{\delta P}\right)_T = \Delta V$$

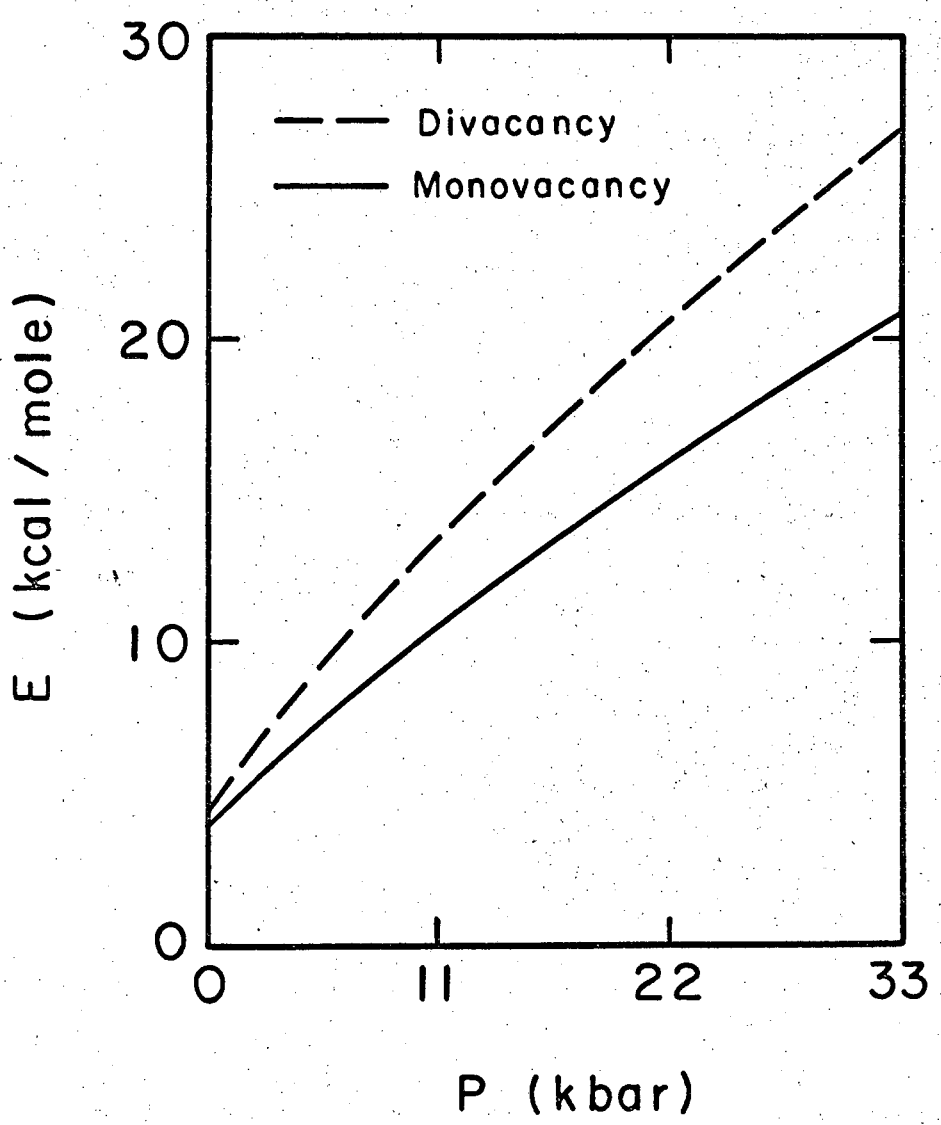

MUB-13062

Fig. 9 Activation energy as a function of pressure for mono- and di-vacancy diffusion.

The energy term used in these calculations is not a true thermodynamic state function and so we calculate the "activation volume" as

$$\Delta V^* = \frac{\Delta E(P_1) - \Delta E(P_2) + P_1\Delta V(P_1) + P_2\Delta V(P_2)}{P_1 - P_2}$$

Using our data for "activation energy" (Fig. 9) we have determined ΔV^* for both mono- and divacancy self-diffusion

$$\Delta V_V^* = 1.2 \text{ atomic volumes}$$

$$\Delta V_{V_2}^* = 1.8 \text{ atomic volumes}$$

No other vacancy type process can have a sufficiently low "activation energy" to agree with the experimental results. However, it would be desirable to calculate the activation energies for exchange, ring, and interstitial mechanisms in solid argon to assure that these do not give suitable "activation energies".

In Section IC we found that the energy required to produce a vacancy adjacent to an impurity atom is dependent on the nature of the impurity atom. The energy required to form a vacancy adjacent to a neon impurity is

$$E_V = 1877 \text{ cal}$$

Using the programs developed for self diffusion we find, for monovacancy diffusion of neon through argon,

$$E_V^\dagger = 305 \text{ cal}$$

The "activation energy" in the Arrhenius expression is then

$$E = E_V^{\dagger} + E_V = 2182 \text{ cal}$$

Similarly for krypton diffusion through argon

$$E_V = 1778 \text{ cal}$$

$$E_V^{\dagger} = 2075 \text{ cal}$$

$$E = 3873 \text{ cal}$$

5. Conclusions

In this Section we have calculated the "activation energy" of self-diffusion in solid argon based on a monovacancy exchange mechanism using an equilibrium approach to the diffusional jump frequency. We have shown that monovacancy exchange gives a value in agreement with experiment[38] for the "activation energy", E, in the Arrhenius expression

$$D = D_o e^{-E/RT}$$

We have also shown that a divacancy exchange mechanism for self-diffusion in solid argon leads to a "frequency factor" greater than that for monovacancy exchange and to a satisfactory value of the "activation energy", and that at high pressure the "activation energy" for divacancy diffusion is much greater than that of monovacancy diffusion.

Finally we have found that for impurity diffusion through argon via a monovacancy mechanism the "activation energy" varies greatly with the nature of the impurity. For divacancy diffusion, the energy of formation of the divacancy is the main term in the "activation energy" and thus the "activation energy" does not vary strongly with the nature of the impurity.

Assuming that the "frequency factor" for a given diffusion mechanism does not vary greatly from self to impurity diffusion, our calculations for argon, krypton and neon indicate that large impurities (e.g., krypton in argon) should diffuse by divacancy mechanism and small impurities by a monovacancy mechanism.

Some experimental data for diffusion in metals are tabulated in Table XII. The self diffusion coefficients are all characterized by large pre-exponentials. For relatively large impurities, the diffusion coefficient "frequency factors" and "activation energies" are roughly equal to the values for self diffusion. However, for relatively small impurities, the "frequency factors" and "activation energies" are drastically reduced from the self diffusion parameters. These experimental results are in agreement with our theoretical prediction that large impurities and bulk atoms diffuse by a divacancy mechanism while small impurities diffuse via monovacancies.

Table XII. Diffusion Coefficients, D, for Face-Centered-Cubic Solids

R is the ratio of the "diameter" of the diffusing atom to that of the atoms in the host lattice where the "diameters" are taken as the nearest neighbor distance in the pure solid. Energies are in cal/mole.

Solid	Diffusing Atom	R	D	Reference
Ar	Ar	1.0	$15\ e^{-4120/RT}\ cm^2/sec$	38
Pb	Pb	1.0	$.28\ e^{-24,200/RT}$	44
Pb	Cu	.73	$7.9\times10^{-3}\ e^{-8020/RT}$	45
Pb	Ag	.82	$4.6\times10^{-2}\ e^{-14,440/RT}$	45
Pb	Au	.82	$2.5\times10^{-3}\ e^{-8700/RT}$	46
Cu	Cu	1.0	$.47\ e^{-47,100/RT}$	47
Cu	Ag	1.12	$.63\ e^{-46,500/RT}$	48
Cu	Au	1.12	$.69\ e^{-49,700/RT}$	48
Cu	Pd	1.08	$1.7\ e^{-54,400/RT}$	49
Ag	Ag	1.0	$.40\ e^{-44,100/RT}$	50
Ag	Au	1.0	$.26\ e^{-45,500/RT}$	51
Ag	Cu	.89	$1.2\ e^{-46,100}$	51
Ag	Pd	.95	$9.6\ e^{-56,700/RT}$	49

E. Surface Dilation

Until now, experimental values have not been obtained for the displacement of the surface layers from the bulk of semi-infinite crystals; such information will probably soon be available from Low Energy Electron Diffraction (LEED) studies. It is desirable to have some theoretical estimation of the order of magnitude of the displacements.

Gazis and Wallis[52] have shown that a one dimensional lattice with nearest and next-nearest neighbor interactions may exhibit a distortion of the lattice spacing at a free surface: the predicted distortion decreases exponentially with distance from the surface.

Shuttleworth[11] has calculated the displacement of the first layer of the (100) surface of argon. Alder et al.[12] have calculated the displacements of the first five layers of the (100) surface of argon; they found that the distortion decreased proportionally to the inverse cube of the distance from the surface.

The values of the coefficients in the Morse potential

$$\phi(r) = D \left\{ e^{-2\alpha(r-r_o)} - 2e^{-\alpha(r-r_o)} \right\}$$

have been tabulated by Girifalco and Weizer[53] for six fcc metals, Ca, Ag, Al, P, Cu, and Ni (Table XIII). Girifalco's evaluation of the Morse potential parameters was based on experimental values of the solid interatomic distance, the heat of sublimation, and the solid compressibility. The Morse potentials obtained give good equations of state but poor elastic constants. We have calculated the displacements, δ_i (Fig. 10) of the first two surface layers of these metals for the (100), (110), and (111) surfaces. For comparison purposes we have also calculated the same displacements for argon using a Lennard-Jones 6-12 potential.[15]

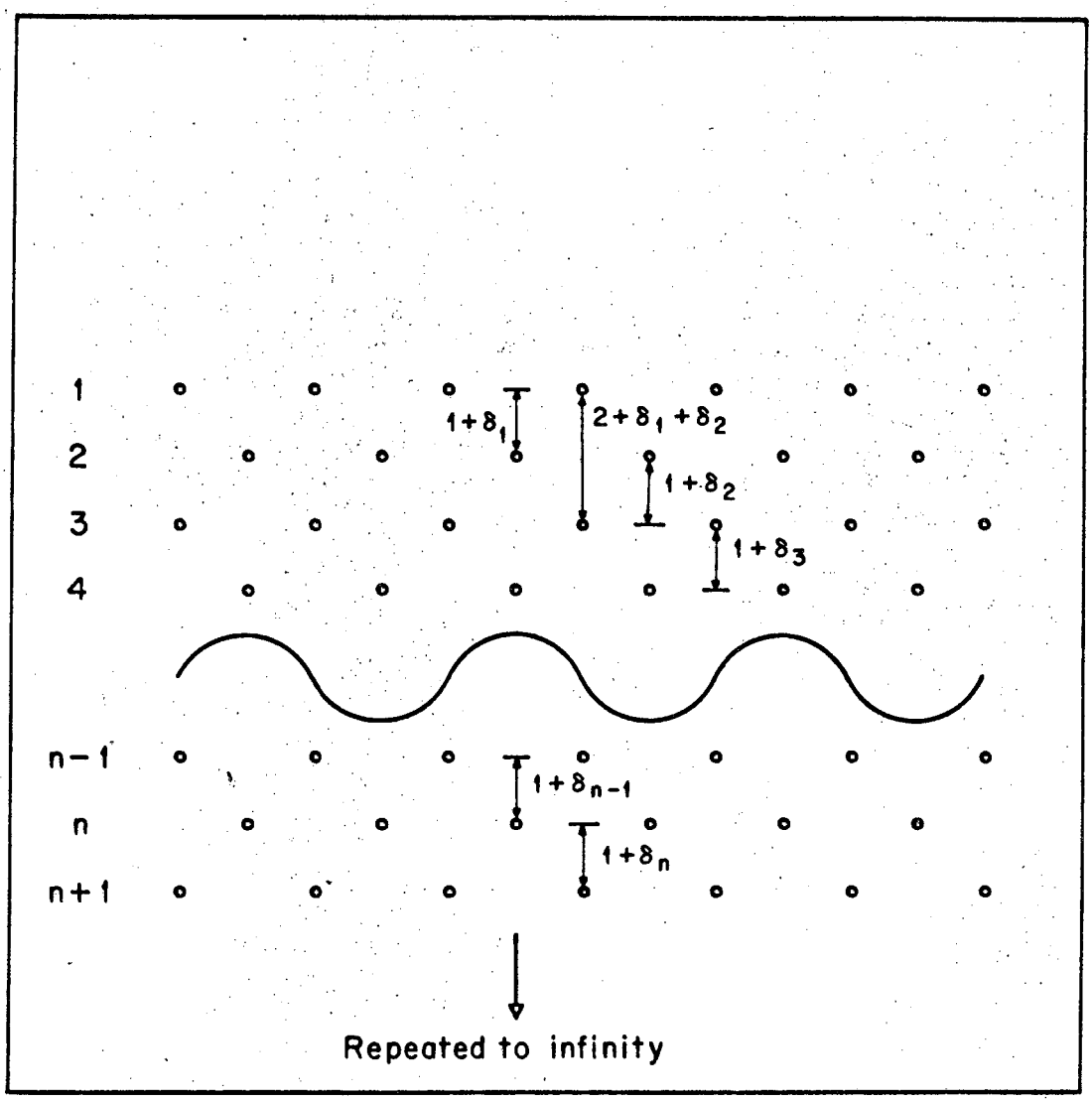

Fig. 10 Schematic diagram of a semi-infinite crystal with displacements indicated.

Table XIII. Parameters of Morse potential

$$\phi(r) = D[e^{-2\alpha(r-r_o)} - 2e^{-\alpha(r-r_o)}]$$

Metal	$\alpha(\text{Å}^{-1})$	$r_o(\text{Å})$	D(ev)
Pb	1.1836	3.733	.2348
Ag	1.3690	3.115	.3323
Ni	1.4199	2.780	.4205
Cu	1.3588	2.866	.3429
Al	1.1646	3.253	.2703
Ca	.80535	4.569	.1623

The expression for the surface energy of the (100) surface with the spacing of the first two planes perpendicular to the surface (z direction) allowed to change by δ_1 and δ_2 and the other planes fixed illustrates the method employed in these calculations, which is that employed by Alder et al.[12] We define $\theta(z + \delta_1)$ by

$$\theta(z + \delta_1) = \sum_{\substack{x,y = -\infty \\ x+y+z = \text{even}}}^{\infty} V(x,y,z + \delta_1)$$

where $V(x,y,z)$ is the potential between an atom at (0,0,0) and an atom at (x,y,z). Then the potential energy of atom in the surface layer is given by

$$E(1) = \theta(0) + \theta(1 + \delta_1) + \sum_{z=2}^{\infty} \theta(z + \delta_1 + \delta_2)$$

with only the first and second layers relaxed. For an atom in the second layer the total energy is

$$E(2) = \theta(0) + \theta(1 + \delta_1) + \sum_{z=1}^{\infty} \theta(z + \delta_2)$$

For an atom in the Nth ($N > 2$) layer the total energy is

$$E(N) = \theta(0) + \theta(N-1 + \delta_1 + \delta_2) + \theta(N-2 + \delta_2) + \theta(N-2) + \sum_{t=1}^{\infty} \theta(z)$$

Adding the energies of all of the atoms in all of the layers gives twice the total binding energy of the system

$$-2E_T = \sum_{N=1}^{\infty} E(N)$$

For a perfect infinite crystal the total binding energy, E_B is given by

$$-2E_B = \lim_{N \to \infty} 2N[\theta(0) + 2 \sum_{z=1}^{\infty} \theta(z)]$$

The surface energy of a crystal is defined as one half the energy required to split an infinite crystal into two semi-infinite crystals

$$E_s = \frac{1}{2}(E_B - 2E_T)$$

$$= \frac{1}{2} \sum_{z=1}^{\infty} z\theta(z) + \sum_{z=2}^{\infty} [\theta(z) - \theta(z + \delta_1 + \delta_2)]$$

$$+ \sum_{z=1}^{\infty} [\theta(z) - \theta(z + \delta_2) + \theta(1) - \theta(1 + \delta_1)]$$

Similar expressions may be developed for more relaxations and other crystal faces.

The surface energy, without allowing for distortion, E_o, was calculated for each case considered by direct summation over a lattice of 2000 atoms. The surface energy was then minimized with respect to the displacements, δ_1, by direct summation of the energy over a lattice of 360 atoms on a CDC 6600 computer.

The surface energies without relaxation, E_o, the displacements, δ_i, and the changes in surface energy due to relaxation, ΔE, are tabulated in Tables XIV, XV, and XVI for the (100), (110), and (111) surfaces respectively. The displacements, δ_i, are given in units of percentage of the normal bulk planar spacing. The values of Alder et al.[12] are included in Table XIV..

The results of Alder et al. are based on direct summation of the energy over a lattice of roughly forty thousand atoms and integration over the remainder of the lattice; our results are based on only 360 atoms. Comparison of Alder's results with ours shows that this small lattice yields good values of δ_1, δ_2, and ΔE. Alder's work shows that consideration of the relaxation of only two surface layers gives good values of the surface energy. It is not necessary to do calculations on large crystals to get reasonable values of the surface energy and surface distortion for solids with short range potentials. Relaxations were found to alter the surface energy by at most 6%. However, consideration of relaxation affects the relative orders of the surface energies per unit area in some cases.

Table XIV

The (100) Surface: Relaxations, δ_1, are given as a percentage of the bulk (100) planar spacing; E is the unrelaxed (100) surface energy; ΔE is the change in surface energy due to relaxation.

Solid	δ_1 (%)	δ_2 (%)	E_o (ergs/cm^2)	ΔE_o (ergs/cm^2)
Ca	12.504	3.587	1034	-68
Ag	6.456	1.259	2508	-72
Al	10.972	2.963	2962	-167
Pb	5.542	.978	1024	-26
Cu	9.669	2.433	4236	-204
Ni	9.121	2.232	5246	-236
Ar	2.604	.623	42.33	-.38
Ar*	2.577	.589	42.86	-.38

*Obtained by Alder et al.[12]

Table XV

The (110) Surface: Relaxations, δ_1, are given as a percentage of the bulk (110) planar spacing; E is the unrelaxed (110) surface energy; ΔE is the change in surface energy due to relaxation.

Solid	δ_1 (%)	δ_2 (%)	E_o (ergs/cm^2)	ΔE_o (ergs/cm^2)
Ca	9.621	2.628	1065	-63
Ag	4.783	.768	2635	-61
Al	8.362	2.099	3063	-153
Pb	4.075	.559	1177	-22
Cu	7.314	1.671	4400	-184
Ni	6.872	1.507	5460	-211
Ar	1.809	.366	44.32	-.30

Table XVI

The (111) Surface: Relaxations, δ_1, are given as a percentage of the bulk (111) planar spacing; E is the unrelaxed (111) surface energy; ΔE is the change in surface energy due to relaxation.

Solid	δ_1 (%)	δ_2 (%)	E_o (ergs/cm^2)	ΔE_o (ergs/cm^2)
Ca	4.297	.899	1046	-31
Ag	1.910	.225	2484	-24
Al	3.667	.709	2985	-71
Pb	1.580	.159	1099	-8
Cu	3.142	.544	4375	-85
Ni	2.927	.490	5258	-93
Ar	.820	.190	40.74	-.14

F. Surface Defects

1. Introduction

A number of investigators have calculated the energy of formation of surface vacancies and the binding energies of excess atoms above the surface for ionic crystals.[54,55] The calculation of the surface energies for ionic crystals is a very difficult problem,[14] thus one cannot expect much exact information from surface defect calculations on ionic crystals.

It is desirable to do extensive calculations on the surface properties of argon in the hope that the results obtained would give some insight into the surface properties of other materials. Potential functions for adsorption of excess atoms onto the surface and for the removal of atoms (both host and impurity) from the perfect surface and information on the configuration of the surface, both perfect and defective, would be useful. The distortion of the perfect (100) surface of argon has been calculated previously.[12]

We have calculated the binding energies of argon and impurity atoms (neon and krypton) above and in the (100) surface plane of argon. Using the high temperature Einstein approximation to calculate the entropy, we estimate the concentration of vacancies in the equilibrium (100) surface of argon at its melting point assuming that the vacancies obey Boltzmann statistics. Though use of our data at the melting point is not justified by our assumptions, it is felt that the results obtained in this way give at least a rough estimate of the surface vacancy concentration at the melting point.

We find, as expected, that the binding energy to the argon surface decreases in the series krypton, argon and neon. We also find, in accord with expectations, that the binding energies of neon and krypton above the

perfect surface are less than in the surface plane. We find that though the relaxations are usually numerically small, they appreciably affect the energy.

2. Calculations

The energy of formation of a vacancy at (0,0,0) in a (100) surface plane without allowing for relaxation is

$$E_o = \sum_{\substack{i+j+k=\text{even} \\ k\geq 0}}{}' V(i,j,k)$$

where the prime (') indicates that the point (0,0,0) is not included in the summation and V(i,j,k) is the potential energy between an atom at (i,j,k) and an atom at (0,0,0). The summation over only lattice points with (i+j+k) = even is the convention adopted by Alder et al.[12] and makes the edge of the unit equal to 2. Allowing the lattice to assume the distortions, δ_k (Table XVII), determined by Alder et al. and allowing the atoms at (1,1,0) and equivalent atoms {(-1,1,0), (1,-1,0) and (-1,-1,0)} to relax to (1-D, 1-D, 0), etc., the energy of formation of the defect may be written as

$$E = \sum_{\substack{i+j+k=\text{even} \\ k\geq 0}}{}' V\left(k,j,k + \sum_{l=0} \delta_l\right)$$

$$+ 4\sum_{\substack{i+j+k=\text{even} \\ k\geq 0}}{}' V\left(i+D,\ j+D,\ k + \sum_{l=0}^{k} \delta_l\right)$$

$$- 4\sum_{\substack{i+j+k=\text{even} \\ k\geq 0}}{}' V\left(i,j,k + \sum_{l=0}^{k} \delta_l\right)$$

$$+ \; 4V(2\text{-}2D,\ 0,\ 0) + 2V(2\text{-}2D,\ 2\text{-}2D,\ 0)$$

$$+ \; 4V(2,0,0) - 8V(D,\ 2\text{-}D,\ 0)$$

$$+ \; 2V(2,2,0) - V(2\text{-}D,\ 2\text{-}D,\ 0)$$

This expression for E was minimized with respect to the relaxation D of atom (1,1,0) by a half interval technique on a CDC 6600 computer. More complicated expressions must be minimized when more relaxations are allowed. Similar expressions may be developed for other types of defects.

Table XVII

Relaxations, δ_i, of the (100) surface of solid argon from Alder et al.[6]

δ_1	δ_2	δ_3	δ_4	δ_5
.025782	.005892	.001981	.000849	.000420

3. Results

The binding energy, E, and relaxations for argon, neon and krypton atoms above the argon surface are given in Table XVIII, as are the binding energies without consideration of relaxation, E_o. The defect is located initially at the point (0,0,0) above a semi-infinite argon crystal with lattice points (i,j,k) subject to $k \geq 1$ and $(i + j + k)$ an even number. An atom at the lattice point (i,j,k) relaxes to the new position $(i - \delta i,\ j - \delta j,\ k - \delta k)$. δi, δj, δk are tabulated.

Configuration and energy of surface vacancies and surface substitution

Table XVIII

The relaxations of the (100) surface of argon with an extra atom above the surface at (0,0,0). The lattice points have coordinates (i,j,k), $k \geq 1$, and are grouped into sets of equivalent points

$(0,0,0)$

$(1,0,1) \equiv (-1,0,1) \equiv (0,1,1) \equiv (0,-1,1)$

$(0,0,2)$

$(2,1,1) \equiv (2,-1,1) \equiv (-2,1,1) \equiv (-2,-1,1)$

$(1,2,1) \equiv (-1,2,1) \equiv (1,-2,1) \equiv (-1,-2,1)$

The point (i,j,k) relaxes to $(i-\delta i, j-\delta j, k-\delta k)$ and $\begin{pmatrix}\delta i\\ \delta j\\ \delta k\end{pmatrix}$ is tabulated for one point of each set of equivalent points.

The binding energy of the extra atom is tabulated without and with relaxation, E_o and E respectively.

	Extra Atom		
	Ar	Ne	Kr
E_o	1355 cal/mole	592 cal/mole	1578 cal/mole
E	1367 cal/mole	687 cal/mole	1682 cal/mole
Points			
$\begin{pmatrix}0\\0\\0\end{pmatrix}$	0 0 .01831	0 0 -.16982	0 0 .06647
$\begin{pmatrix}1\\0\\1\end{pmatrix}$	-.00319 0 -.00558	-.00196 0 -.00167	-.00378 0 -.00752
$\begin{pmatrix}0\\0\\2\end{pmatrix}$	0 0 .00255	0 0 .00249	0 0 .00252
$\begin{pmatrix}2\\1\\1\end{pmatrix}$	.00035 -.00017 .00188	-.00001 -.00028 .00117	.00054 -.00010 .00226

impurities are tabulated in Table XIX. Here again the defect is located initially at (0,0,0); the bulk atoms now are at points (i,j,k) subject to $k \geq 0$, (i + j + k) even. The atom at (i,j,k) relaxes to ($i - \delta i$, $j - \delta j$, $k - \delta k$) and (δi, δj, δk) is tabulated. The binding energy of substitutional impurities is relative to the impurity atom infinitely removed from a surface with a vacancy.

In all cases sufficiently many relaxations were calculated to assure convergence of the energy of the defect to .05%.

The relaxations of the lattice around an extra argon atom above the surface are illustrated in Fig. 11 (top view) and Fig. 12 (side view). The nearest neighbors to the extra atom relax towards the bulk .6% from their normal surface positions and outwards tangentially to the surface .3%. The distance between the extra surface atom and its nearest neighbors was found to be roughly equal to the distance between first and second layer atoms in the perfect relaxed surface. The second nearest atoms to the extra atom (in the second layer of the lattice) relax upwards. The second nearest neighbors (in the surface layer) to the extra atom relax in such a way as to decrease their distance to the defective site but increase their separation from the relaxed nearest neighbors. This behavior is similar to that noted previously for the relaxation of the atoms around an internal defect (Section I-C).

With a neon atom above the surface the relaxations of the nearest neighbors are smaller (.2% downwards and .2% outwards) while for krypton they are larger (.8% downwards and .4% outwards).

It is interesting to note that in the fully relaxed situation, an extra neon atom lies closer to the bulk than an extra argon which, in turn, lies closer than an extra krypton atom.

Table XIX

The relaxations of the (100) surface of argon with a defect (vacancy of substituent) in the surface at (0,0,0). The lattice points have coordinate (i,j,k), $k \geq 0$, and are grouped into sets of equivalent points

(0,0,0)
(1,1,0) ≡ (1,-1,0) ≡ (-1,1,0) ≡ (-1,-1,0)
(0,1,1) ≡ (0,-1,1) ≡ (1,0,1) ≡ (-1,0,1)
(2,0,0) ≡ (-2,0,0) ≡ (0,2,0) ≡ (0,-2,0)
(0,0,2)

The point (i,j,k) relaxes to (i-δi,j-δj,k-δk) and $\begin{pmatrix}\delta i\\ \delta j\\ \delta k\end{pmatrix}$ is tabulated for one point of each set of equivalent points.

The binding energy of the substituent atom (or surface binding energy of argon in the case of the vacancy) is tabulated without and with relaxation, E_o and E respectively.

	Defect		
	Vacancy	Ne	Kr
E_o	2627 cal/mole	1134 cal/mole	3081 cal/mole
E	2603 cal/mole	1290 cal/mole	3160 cal/mole
Points			
$\begin{pmatrix}0\\0\\0\end{pmatrix}$	* * *	0 0 -.18131	0 0 .06060
$\begin{pmatrix}1\\1\\0\end{pmatrix}$	.01589 .01589 .00299	.02682 .02682 -.00009	-.013061 -.013061 .00218
$\begin{pmatrix}0\\1\\1\end{pmatrix}$	0 .00265 .00110	0 .00181 -.00453	0 -.00004 .00479

Table XIX (Cont.)

	Defect		
	Vacancy	Ne	Kr
E_o	2627 cal/mole	1134 cal/mole	3081 cal/mole
E	2603 cal/mole	1290 cal/mole	3160 cal/mole
Points			
$\begin{pmatrix}2\\0\\0\end{pmatrix}$	-.00468 0 .000625	-.00249 0 -.00103	.00131 0 .00250
$\begin{pmatrix}0\\0\\2\end{pmatrix}$	0 0 -.00317	0 0 -.00411	0 0 .00317

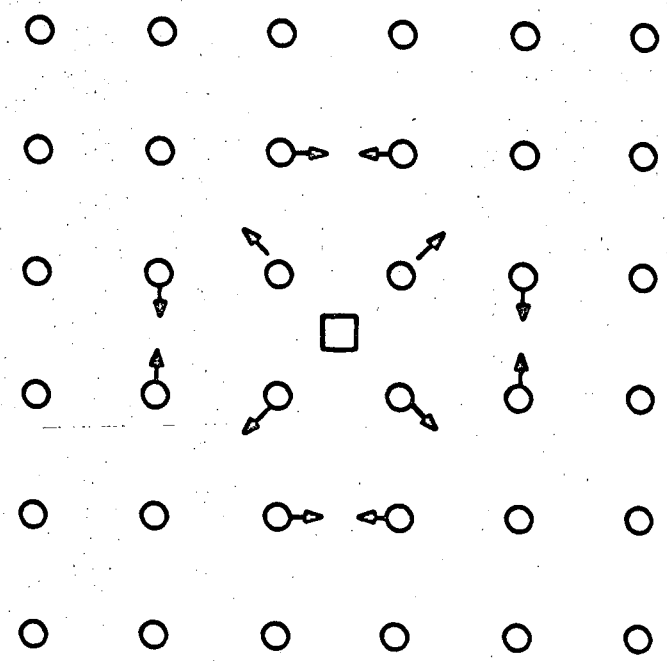

MUB-13063

Fig. 11 Top view of the relaxations of the surface layer with an excess argon atom above it. Arrows indicate the directions of the displacements from the normal positions. The excess atom is represented by a square (□).

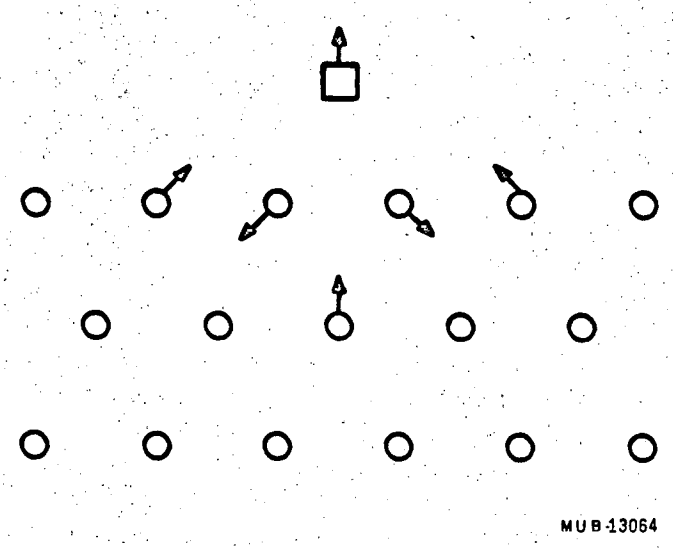

Fig. 12 Side view of the relaxations of the surface layer with an excess argon atom above it. Arrows indicate the directions of the displacements from the normal positions. The excess atom is represented by a square (□).

With a vacancy in the surface, the nearest neighbors to the defect are displaced towards the center of the vacancy (Fig. 13). Krypton substituted in the surface plane (Fig. 14) displaces its nearest neighbors away from the defect; the krypton atom is displaced 6% up from the normal argon location in the crystal surface. A neon substituent in the plane affects its nearest neighbors like the vacancy but the neon atom is displaced 18% towards the bulk of the crystal from the normal argon site.

The direction and magnitude of the displacements are attributable to the sizes of the impurity atoms; argon is larger than neon and smaller than krypton.

With the computed binding energies it is possible to calculate the energy of formation of a vacancy in an argon surface. This was done by assuming that the relevant process involves the removal of a surface atom to a position above the surface and isolated from any other defects. Using the high temperature Einstein approximation to compute the entropy, we have calculated the free energy of formation of a mole of vacancies to be

$$\Delta F = 1236 - 3.58\ T \text{ cal}$$

when relaxations are considered and

$$\Delta F = 1272 - 3.58\ T \text{ cal}$$

without relaxation. This implies that at the melting point of argon there is one vacancy for each three hundred sites on the ideal flat (100) surface or 2×10^{12} per cm^2 of surface.

With slight modification of the programs developed for calculation of the energy of surface defects, we were able to calculate the potential

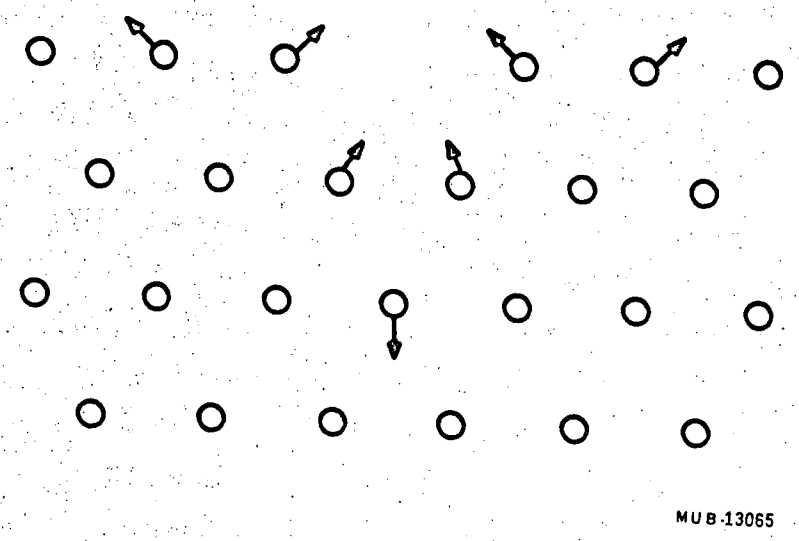

Fig. 13 Side view of the relaxations of the surface layer with a vacancy in the surface. Arrows indicate the directions of the displacements.

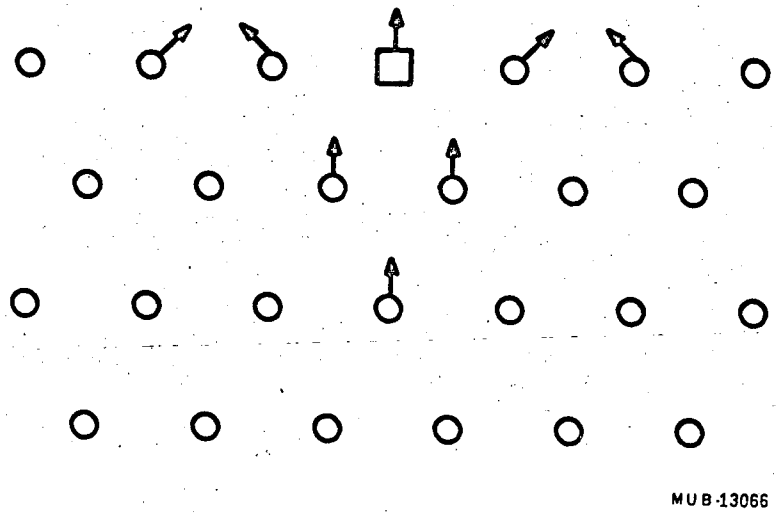

MUB-13066

Fig. 14 Side view of the relaxations of the surface layer with a krypton atom substituted in the surface plane. Arrows indicate the directions of the displacements from the normal positions. The krypton atom is represented by a square (□).

curves for binding of an atom to the lattice, both at a point above the surface and at a normal surface position.

Figures 15 and 16 show the potential curves for binding of neon, argon, and krypton atoms in the surface plane and above it. As expected, the krypton potential curves have the deepest wells and are the widest.

4. Conclusions

The distortion of the crystal surface around a defect is small in most cases but appreciably alters the energy of the defect and is not neglectable in the calculation of surface properties.

Distance of excess atoms above the surfaces increases in the series neon, argon, and krypton. A neon atom substituted in the argon surface is displaced towards the bulk from the normal position while a krypton atom is displaced away from the bulk.

The binding energies of atoms in the surface plane are greater than those of atoms in normal lattice sites above the surface plane.

It was found that the free energy of formation of a mole of vacancies in an argon surface is

$$\Delta F = 1236 - 3.58\ T \text{ cal}$$

which implies that at the melting point of argon there is one vacancy for each three hundred sites on the ideal (100) crystal surface or 2×10^{12} vacancies per cm^2 of surface.

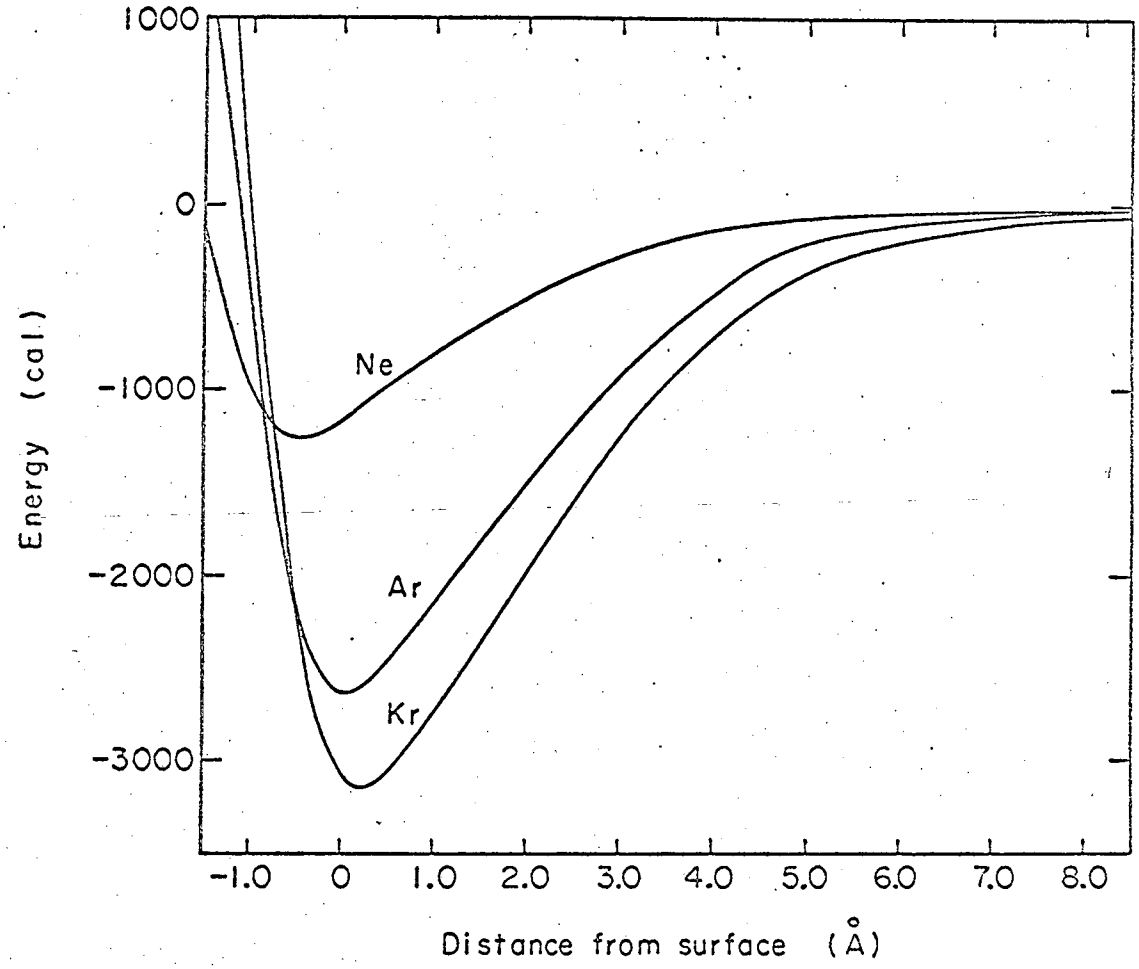

Fig. 15 The potential curves for binding of neon, argon, and krypton atoms in the (100) surface of argon with relaxation allowed.

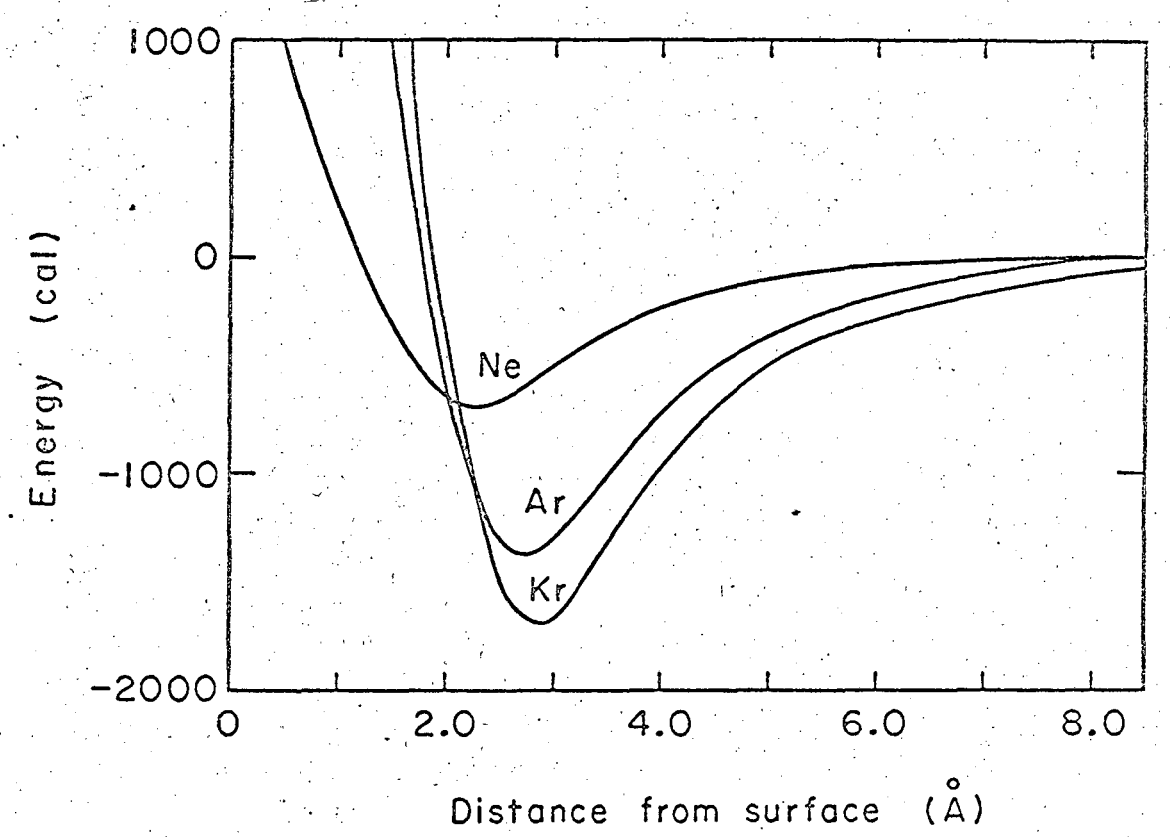

Fig. 16 The potential curves for binding of neon, argon, and krypton atoms above the (100) surface of argon with relaxation allowed.

II. THE FERMI MOMENTUM OF ALUMINUM FROM 0 TO 100 KILOBARS

A. Introduction

In order to understand solids information is required about their electronic states. A number of experimental techniques have been developed for the study of the details of the electronic structure of solids.[56] Most of these techniques require very low temperatures.

Information about the properties of solids at very high pressures is essential for testing theories of solids since this is the only manner in which the inter-atomic distance can be varied. Unfortunately low temperatures, ~4°K, are required for most studies of the electronic structure of metals. This requirement has restricted the investigations to relatively low pressures.[57] Positron annihilation is a tool that has been used for the study of the distribution of the momentum of the conduction electrons.[58] Positron annihilation can be employed at room temperature, which is low compared to the characteristic Fermi temperature of the conduction electrons (10,000 - 50,000°K). Positron annihilation is not as precise or as well understood as those techniques available at very low temperatures; however, it is useful for obtaining some information about the electronic structure of metals and can be used at room temperature where very high pressures are attainable.

We have studied positron annihilation in aluminum in the range of 0 to 100 kbars at room temperature. Aluminum was chosen for this study since it is known not to exhibit any phase transition in the region of interest, and the results are simply interpretable.

From the positron annihilation data we have obtained the variation of the Fermi momentum with pressure. It was found that the Fermi momentum of aluminum increases with pressure in accordance with the prediction of

the free electron model.

Melz[59] has studied the detailed topology of the Fermi surface of aluminum to 7 kbars using the de Haas-van Alphen effect. He found that the Fermi surface does not expand isotropically with compression and attributed this to a change in the band gaps. We will show that Melz's results are consistent with the present work, as the accuracy of this experiment is not nearly great enough to see the effect observed by Melz.

B. Theory

1. Electrons in Metals

A metal can be regarded as a sea of conduction electrons moving in the periodic field of the ion cores of the metal atoms. The electrons interact with each other and with the cores and the cores interact with each other. For such a system a Hamiltonian may be written,

$$\mathcal{H} = \mathcal{H}_{\text{electron-electron}} + \mathcal{H}_{\text{electron-ion}} + \mathcal{H}_{\text{ion-ion}}$$

when

$$\mathcal{H}_{\text{electron-electron}} = \sum_i \frac{p_i^2}{2m} + \frac{1}{2} \sum_{i \neq j} \frac{e^2}{|r_i - r_j|}$$

$$\mathcal{H}_{\text{electron-ion}} = \sum_{i,j} v(r_i - R_j)$$

$$\mathcal{H}_{\text{ion-ion}} = \sum_i \frac{p_i^2}{2M} + \frac{1}{2} \sum_{i \neq j} V(R_i - R_j)$$

and where the lower case letters refer to the electrons and capitols to the ion cores. Detailed examination of this Hamiltonian is given in a number of texts.[60]

a. Free Electron Model. In the free electron approximation all terms in the Hamiltonian are neglected except the kinetic energy of the electron so that

$$\mathcal{H} = \sum_i \frac{p_i^2}{2m}$$

This reduction of the Hamiltonian corresponds to the following physical assumptions:

1. The motions of the ion cores are neglectable.
2. Interactions of electrons with the ion cores are neglectable.
3. Electron-electron interactions are neglectable.

With these assumptions, the metal is represented as a set of non-interacting electrons travelling in a uniform positive charge. This picture of metals is called the free electron model. An excellent simple description of this model and of the deviations of real metals from this model is available in Electrons in Metals by Ziman.[61] This reduced Hamiltonian is merely that of a free particle and the details of its solution with appropriate boundary conditions is available in most standard texts.[62]

The solutions for the free particle Hamiltonian are plane waves

$$\psi_{\underline{k}} = e^{i\,\underline{k}\cdot\underline{r}}$$

and have energy

$$E(\underline{k}) = \frac{\hbar\, k^2}{2m} \equiv \frac{p_k^2}{2m}$$

The surfaces of constant energy are spheres in $\underline{k}$ space and the density of allowed points in $\underline{k}$ space is $V/8\pi^3$ where V is the volume of the lattice.

Electrons are Fermions and so obey Fermi-Dirac statistics. The average occupation number of an electron state is

$$f(E) = \frac{1}{e^{(E-E_F)/kT} + 1}$$

where E_F is a characteristic energy, the Fermi energy. At zero temperature, $f(E)$ is exactly unity for $E < E_F$ and zero for $E > E_F$. All states with energy lower than the Fermi energy are occupied at 0°K and all states with higher energy are empty. At finite temperatures a few electrons are excited to just above the Fermi energy.

Each electron state may hold two electrons of opposite spin. If there are Z conduction electrons per unit cell and N is the number of unit cells per unit volume, then all electron states must be filled at 0°K up to the state with wave number k_F given by

$$k_F = (3\pi^2 ZN)^{1/3}$$

The constant energy sphere in wave number space with radius k_F is called the Fermi surface and the Fermi energy is given by

$$E_F = \frac{\hbar k_F^2}{2m}$$

In momentum space the Fermi momentum is

$$p_F = \hbar\left(\frac{3\pi^2 Z}{V}\right)^{1/3}$$

where V is the volume of the unit cell.

The free electron model of metals predicts values of the Fermi momentum which are in reasonable agreement with experimental data (Table XX); it also predicts that as a metal is compressed, the Fermi

momentum should be linear in $V^{-1/3}$.

Table XX. The Fermi momentum of various metals as predicted by the free electron model and measured by Lang[63] by positron annihilation. m is the mass of an electron and c the velocity of light.

Metal	Computed p_F ($mc \times 10^{-3}$)	Measured p_F ($mc \times 10^{-3}$)
Li	4.27	4.3
Na	3.50	3.6
Be	7.48	7.4
Mg	5.27	5.3
Al	6.74	6.7
Ge	6.69	6.8
Sn	6.29	6.4
Bi	6.21	6.1

The free electron model neglects electron-electron interactions. Luttinger[65] has considered the electron interactions in a sea of electrons. He found that the Fermi surface is well defined for interacting electrons and is identical to that for free electrons; however he also showed for interacting electrons that at 0°K there are occupied electron states with larger momentum than the Fermi momentum.

b. Nearly Free Electron Model. The free electron model of a metal is not an exact representation. An electron does not see a constant potential; the ion cores of the lattice are seen as a periodic potential and we may write the Hamiltonian as

$$\mathcal{H} = \sum_i \frac{p_i^2}{2m} + \sum_{i,j} v(r_i - R_j)$$

This Hamiltonian neglects electron-electron interactions and all motion of the ion cores. As an approximation we may regard the electron-ion interaction as a perturbation on the free electron states

$$\psi_{\underline{k}} = e^{i\,\underline{k}\cdot\underline{r}}$$

This perturbation treatment is known as the nearly free electron model and the details of this model may be found in standard texts.[62] We give only the results of the nearly free electron model.

In the nearly free electron model the energy as a function of $\underline{k}$ is discontinuous at the zone boundaries but is close to the free electron values except near the zone boundaries (Fig. 17). The regions in which $E(\underline{k})$ is continuous in $\underline{k}$ are known as electron bands. The Fermi surface in the nearly free electron model is still a surface of constant energy in $\underline{k}$ space. However, as the energy is not as simply related to the wave vector $\underline{k}$ as in the free electron model, the Fermi surface will generally not be spherical in $\underline{k}$ space. For nearly free electrons the Fermi surface is nearly spherical and one may define the Fermi momentum k_F as the average momentum at the Fermi surface. If the band gaps are small (the electrons are nearly free) the Fermi momentum defined in this way is very close to that predicted by the free electron model.

Though the Fermi momentum is not as simply defined in the nearly free electron model as in the free electron model, the effect of isotropic compression on the electronic states of a cubic lattice is readily understood. Assuming that (1) the compression of the lattice

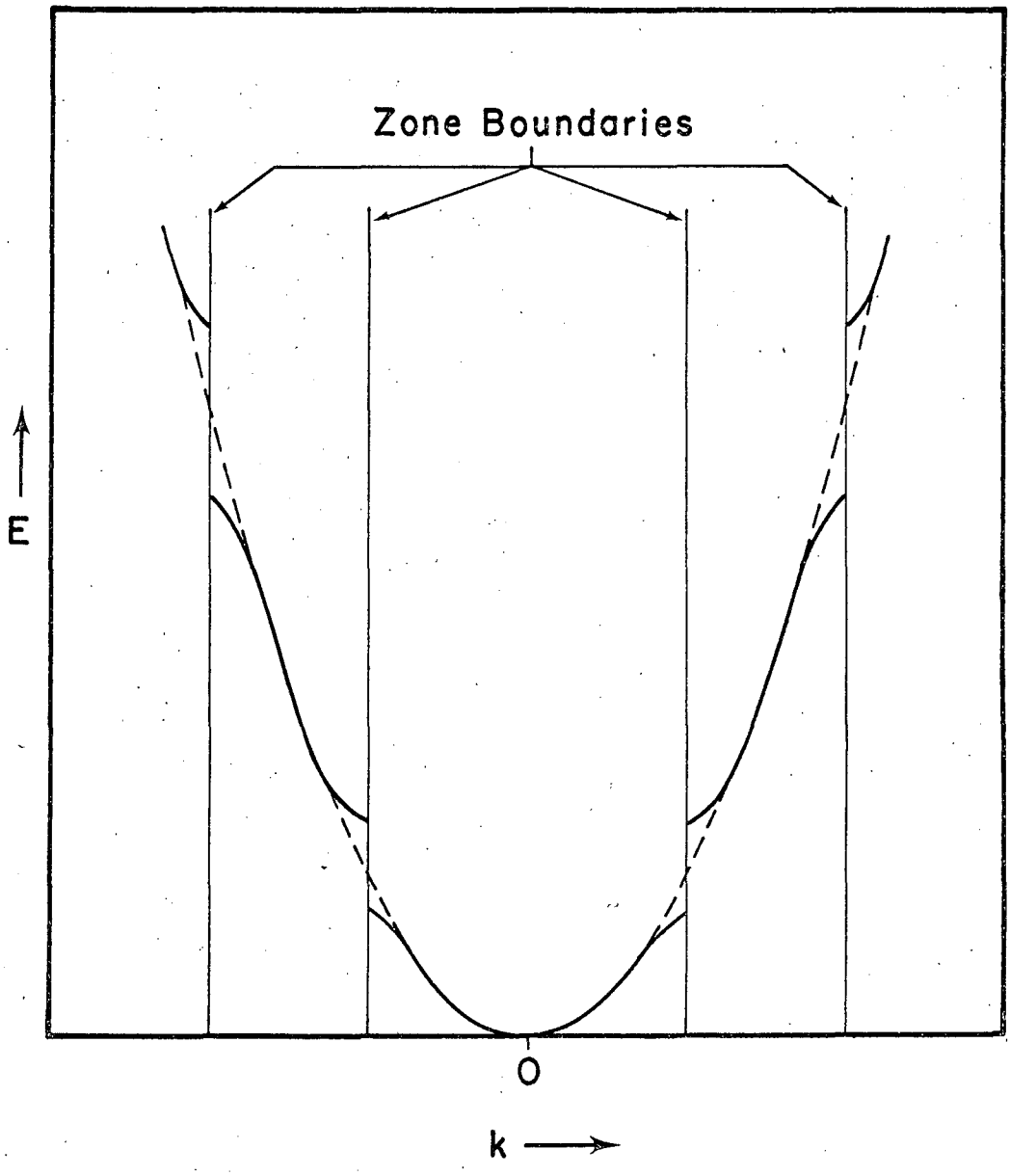

XBL 674-1394

Fig. 17 The electron energy as a function of wave number k. The dashed curve is predicted by the free electron model and the solid curve by the nearly free electron model.

is isotropic and (2) that the band gaps are pressure independent the reciprocal lattice in $\underline{k}$ space is uniformly expanded. The density of allowed wave numbers is decreased and the Fermi surface is expanded isotropically. The rate of expansion of the Fermi surface is equal to that of $\underline{k}$ space itself and so the qualitative features of the electron states near the Fermi surface are not altered except that their energy is increased. The nearly free electron model predicts that, under isotropic compression, the detailed topology of the Fermi surface is not altered and the Fermi surface expands isotropically and proportionately to $(V_o/V)^{1/3}$ as in the free electron model. The free electron and nearly free electron models differ only in that the latter predicts allowed energy bands.

If the band gaps are pressure dependent the Fermi surface does not expand isotropically under isotropic compression. Melz[59] used pressure dependence of the band gaps to explain the de Haas-van Alphen effect studies on aluminum to 7 kbars. We will show that our results are not inconsistent with the work of Melz.

2. The Fermi Surface of Aluminum

Solutions of the wave equation in a periodic lattice can be expressed in the form

$$\psi_{\underline{k}}(r) = u_{\underline{k}}(r)\ e^{i\,\underline{k}\cdot\underline{r}}$$

where $u_{\underline{k}}$ has the periodicity of the lattice and $\underline{k}$ is a vector in the reciprocal space of the lattice. As

$$e^{i\,\underline{k}\cdot\underline{r}} = e^{i(\underline{k}+\underline{K})\cdot\underline{r}}$$

where $\underline{K}$ is a lattice vector in the reciprocal space, it is usually most convenient to examine the behavior of the electron energy as a function of $\underline{k}$ in some unit cell of $\underline{k}$ space. The conventional unit cell used in most solid state electron or lattice dynamics work is the so-called Wigner-Seitz unit cell. The Wigner-Seitz cell is the smallest cell bounded by the planes which perpendicularly bisect the vectors connecting a lattice point in $\underline{k}$ space with the other lattice points. The Wigner-Seitz unit cell of the reciprocal space of aluminum (fcc) is shown in Fig. 18. This unit cell is known as the first Brillouin zone and the density of states in $\underline{k}$ space is such that the first zone can contain exactly two electron states per atom in the lattice. The second Brillouin zone is the next larger cell bounded by the planes constructed as perpendicular bisectors of the lattice vectors and does not include the part of $\underline{k}$ space contained in the first zone. The second Brillouin zone of aluminum is shown in Fig. 19. Any point, $\underline{k}$, in the second (or higher) zone can be expressed as

$$\underline{k} = \underline{k}_o + \underline{K}$$

where $\underline{k}_o$ lies in the first zone and $\underline{K}$ is a lattice vector. As it is often difficult to visualize higher Brillouin zones, it is conventional to draw energy surfaces in reduced Brillouin zones by reducing the higher zone to the first by the above relation. We will follow this convention and draw reduced zones when speaking of electron states.

Harrison[66] has obtained the Fermi surface of aluminum by constructing an initial trial surface from the free electron model and distorting this surface to give agreement with the de Haas-van Alphen effect and

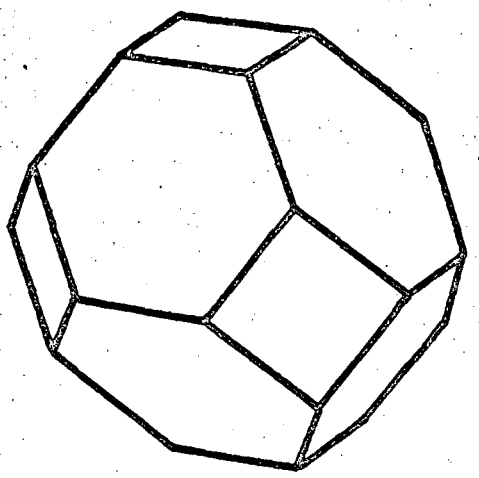

XBL 674-1397

Fig. 18 The Wigner-Seitz unit cell of the reciprocal space of aluminum (the first Brillouin zone). Reproduced from Ref. 65 by permission of McGraw-Hill Book Company.

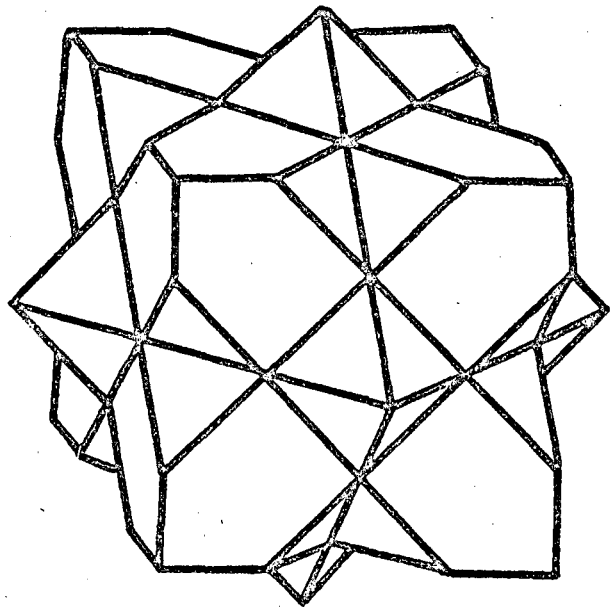

XBL 674-1398

Fig. 19 The second Brillouin zone of aluminum. Reproduced from Ref. 65 by permission of McGraw-Hill Book Company.

anomalous skin effect data. He has found that the corrected Fermi surface is nearly identical to that predicted by the free electron model.

In aluminum the first Brillouin zone in $\underline{k}$ space is completely filled with electrons. The second zone is almost half full and the occupied states (below the Fermi level) are bounded by a single closed surface; the third zone is almost empty and the occupied states are bounded by a multiply connected surface; and the fourth zone has small pockets of electrons. The four (reduced) zones for aluminum predicted by the free electron model are shown in Fig. 20 and the third zone Fermi surface obtained by Harrison[66] is shown in Fig. 21.

Ashcroft[67] has used two Fourier coefficients, V_{111} and V_{200}, of a weak pseudo-potential for an orthoganalized plane wave (OPW) calculation of the Fermi surface of aluminum. He adjusted the coefficients to obtain a fit with de Haas-van Alphen effect data at zero pressure. Ashcroft's third zone Fermi surface differs from that of Harrison in that the internal ring of the Fermi surface, Fig. 21, disappears leaving the arms of the monster disconnected. In the second zone Ashcroft's surface is like that for free electrons.

As the Fermi surface of aluminum at zero pressure is nearly that predicted by the free electron model, we would expect that under pressure the Fermi surface of aluminum should expand isotropically and proportionally to $(V_o/V)^{1/3}$. Melz[59] has studied the third zone Fermi surface of aluminum to 7 kbars using the de Haas-van Alphen effect. He found that the surface does not expand isotropically and, in fact, contracts in one part of the third zone. Melz attributed this to a change in the band gaps with pressure and was able to fit his data using Ashcroft's pseudo-potential coefficients and their pressure derivatives obtained from Harrison's[68] model for the pseudo-potential form factor.

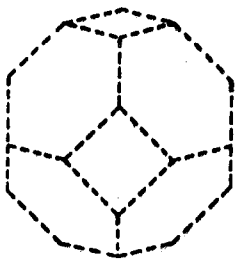

First Zone

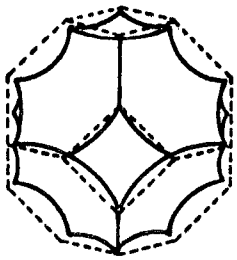

Second Zone

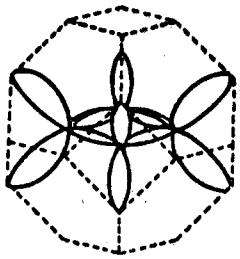

Third Zone

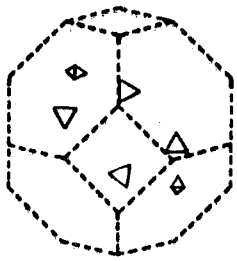

Fourth Zone

XBL 674-1393

Fig. 20 Free electron Fermi surface of aluminum reproduced from Ref. 66 with the permission of the author.

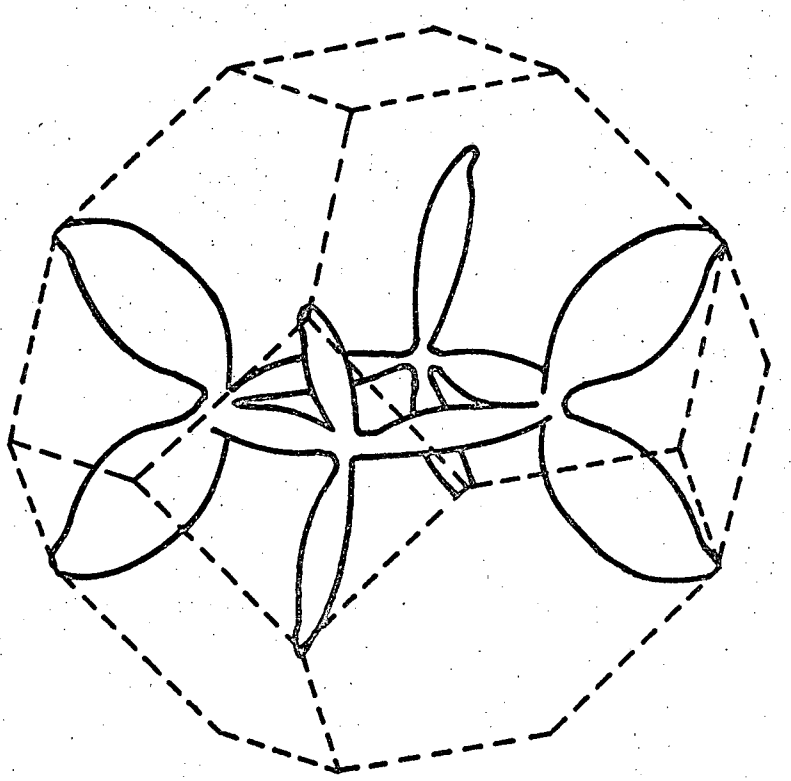

XBL 674-1392

Fig. 21 The third zone Fermi surface of aluminum obtained by Harrison and reproduced from Ref. 66 with the permission of the author.

3. Positron Annihilation

When a positron is introduced into a metal lattice it annihilates with an electron of the lattice. The annihilation may occur either from a triplet state, leading to three γ's, or from a singlet, giving two γ's. The half life of the positron is long compared with the time required for it to be thermalized and it is thought that most of the observed annihilation is between thermal positrons and conduction electrons.[70] It is the two quantum annihilation which is usually studied.

Two quantum positron annihilation is studied by observing the distribution of annihilation radiation as a function of angle between the γ's. A schematic representation of the experimental set up is shown in Fig. 22. The sample is located between two detectors and the coincident count rate as a function of angle between the detectors is obtained. This does not give the true angle between the γ's but only the projection of this angle on the plane of the counters and the source. The count rate as a function of this (projected) angle is referred to as the annihilation spectrum. In practice the counters are usually distant from the source and have long narrow windows in order to give high angular resolution.

If the positron electron pair is at rest prior to the annihilation the two γ's are released back to back and are observed at 180°; they each have energy equal to the rest mass of the electron (or positron, .511 meV), and have a momentum of mc where m is the mass of a free electron and c the velocity of light. If the positron electron pair has non-zero momentum, the annihilation γ's will generally not be observed back to back but at some angle $180° - \theta$ and generally will not have energy exactly equal to .511 meV.

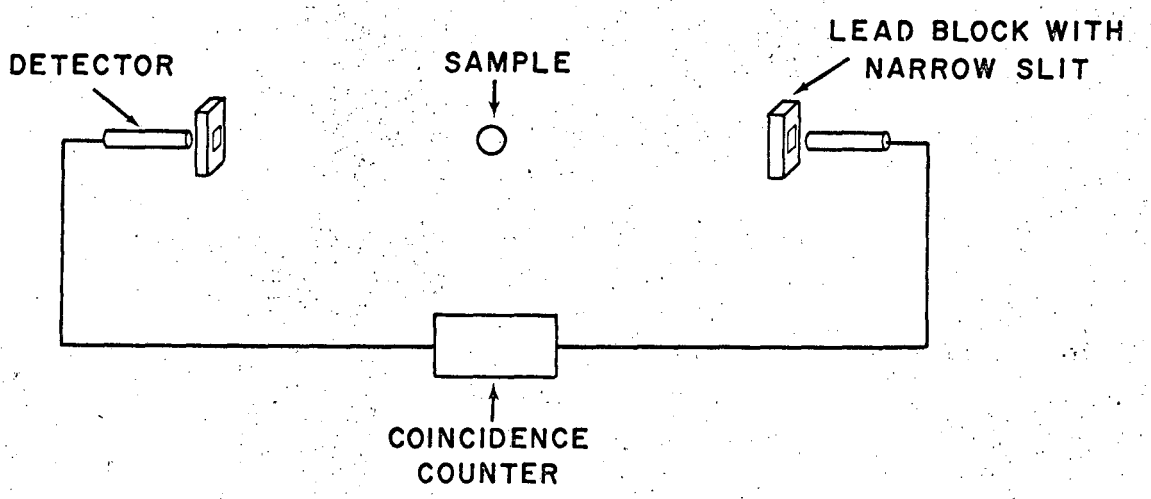

XBL 674-1399

Fig. 22 A schematic representation of an apparatus for studying positron annihilation. When γ's are registered coincidentally by the two defectors, a count is registered.

The laboratory coordinates are defined by the plane of the detector slits when the detectors are at 180° to each other; the z direction is taken perpendicular to this plane. Experimentally we observe one component of the electron-positron momentum, p_z. In the moving coordinates of the electron positron pair the γ's are emitted at 180° and have momentum mc. The momentum of the electron positron pair in the laboratory coordinates, which is small compared to mc, is added to that of the γ's. We observe the angle, θ, between the γ's which is related to p_z by (Fig. 23)

$$\sin \theta = \frac{p_z}{mc}$$

Experimentally we observe one component of the momentum of the electron positron pair, p_z. Assuming that the electron-positron pairs have momentum distribution $\rho(p)$ the distribution of p_z is

$$\rho_o(p_z) = \int \rho(\underline{p})\, dp_x\, dp_y$$

$$= \int_o^\infty \rho(p)\, 2\pi\, pdp$$

where

$$p = \sqrt{p_x^2 + p_y^2}$$

Letting

$$p^2 + p_z^2 = p^2$$

$$\rho_o(p_z) = 2\pi \int_{p_z}^\infty \rho(p)\, pdp$$

For free electrons at 0°K, assuming the positrons have zero momentum

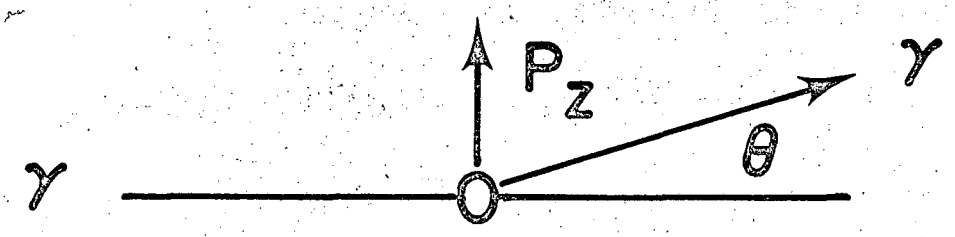

XBL 674-1395

Fig. 23 Two γ's are released back to back in the moving coordinates of electron-positron pair and are observed in the laboratory at angle θ where

$$\sin \theta = \frac{p_z}{mc}$$

and p_z is the z component of the momentum of the electron-positron pair.

$$\rho(p) = A\,p^2 \qquad (p \leq p_F)$$

$$= 0 \qquad (p < p_F)$$

where p_F is the Fermi momentum. Substituting this into the above

$$\rho_o(p_z) = B(p_F^2 - p_z^2) \qquad (p_z \leq p_F)$$

$$= 0 \qquad (p_z > p_F)$$

The count rate at angle θ , $N(\theta)$, is proportional to $\rho_o(p_z)$ where

$$\sin\theta = \frac{p_z}{mc}$$

Thus the positron annihilation spectrum for free electrons at 0°K has the form

$$N(\theta) = C\,(\theta_F^2 - \theta^2) \qquad (\theta \leq \theta_F)$$

$$= 0 \qquad (\theta > \theta_F)$$

where θ_F is the angle that corresponds to the Fermi momentum

$$\sin\theta_F = \frac{p_F}{mc}$$

This annihilation spectrum is a parabola.

On the basis of the assumption (1) the electron momentum distribution is that predicted by the free electron model, (2) the electron momentum distribution is not perturbed by the positron, (3) the positron is thermal, and (4) the probability of annihilation of a positron with an electron is independent of the momentum of the electron, then the positron annihilation spectrum of a metal would be a central parabola

which extrapolates to zero at the Fermi momentum, and would have a small tail at large angles corresponding to the excitation of electrons above the Fermi level at room temperatures. This is observed for a number of metals (Fig. 24a); however the tails observed are much larger than those expected for free electrons with the Fermi-Dirac distribution. It is believed that the positrons are thermalized prior to annihilation;[69] however it has been suggested that the positron has a large effective mass or temperature higher than the lattice temperature, and this gives rise to greater intensity in the tail.[70] Luttinger[64] has shown that the distribution of interacting electrons in momentum space has a larger tail than that expected for free electrons. This larger tail in the electron distribution could give a greater intensity in the tail of the positron annihilation spectrum.

Positron annihilation has been studied in a number of metals and it is well known that the two quantum annihilation of positrons in the alkali metals, alkaline earths, and aluminum is characterized by a central parabola with a tail at large angles[63] (Fig. 24a). The annihilation spectra of the transition metals have been found to be less well characterized.(Fig. 24b).

For free electrons at 0°K the maximum momentum is p_F, the Fermi momentum. For positrons with zero momentum the maximum momentum of an electron-positron pair is also p_F. Thus the maximum angle, θ_F, at which coincident γ's could be observed is given by

$$\sin \theta_F = \frac{p_F}{mc}$$

Though the tails of the observed annihilation spectra are not fully understood, it is well known that if the central portion of the

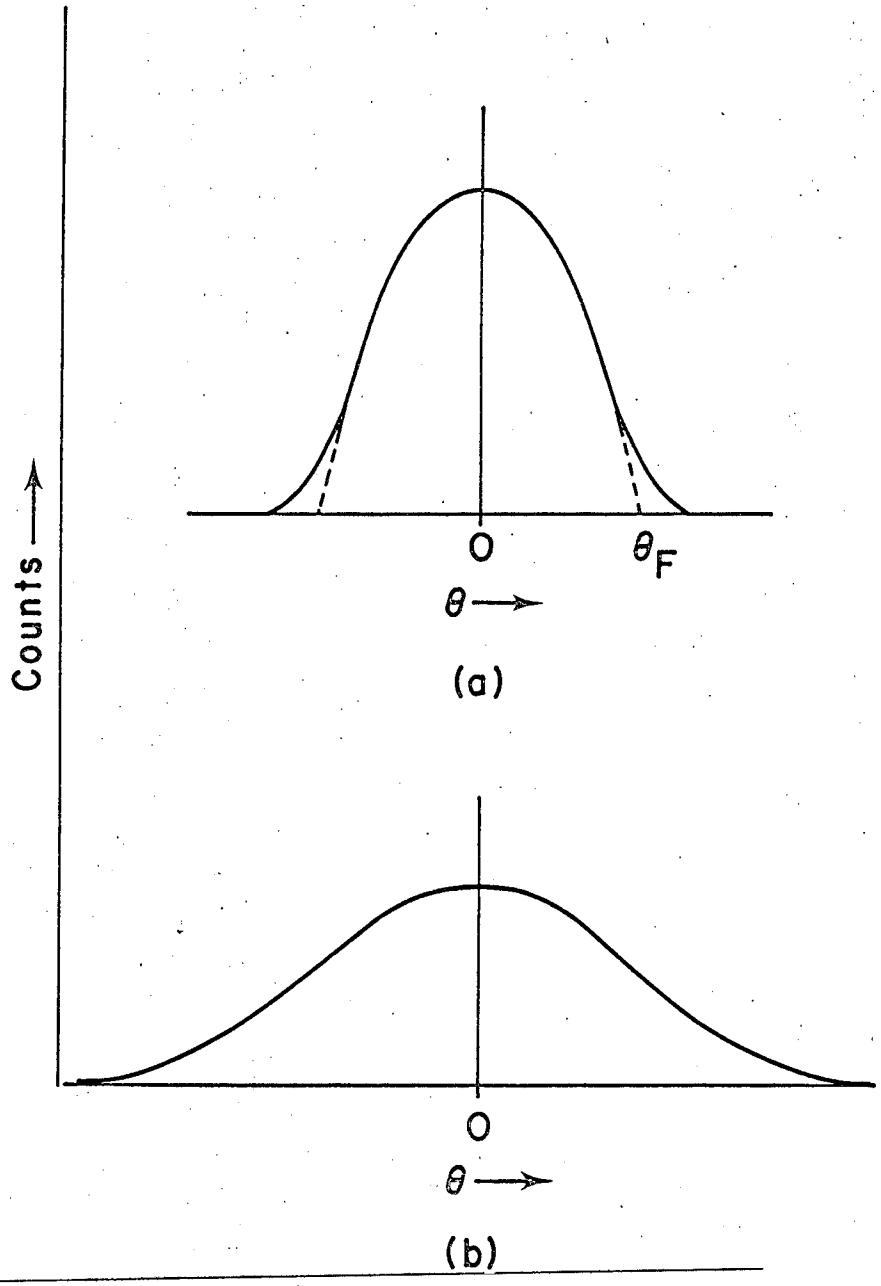

XBL 674-1400

Fig. 24 (a) The positron annihilation spectrum of alkali metals, alkaline earths, and aluminum. The angle at which the central parabola extrapolates to 0, θ_F, is related to the Fermi momentum by

$$\sin \theta_F = \frac{p_F}{mc}$$

(b) the positron annihilation spectrum of positron metals

annihilation spectrum is fit with a parabola, then the angle at which the central parabola extrapolates to zero (Fig. 24a) corresponds to electrons having momentum equal to the Fermi momentum, determined by other techniques.[63] This indicates that experimental values of the Fermi momentum obtained by positron annihilation are meaningful and that a study of the change of the positron annihilation spectrum with pressure should yield the volume dependence of the Fermi momentum.

C. Experimental

We used 500μc of Na^{22} in the form of NaCl as the source of positrons. The NaCl was placed between two 1/8" diameter discs of $\frac{1}{2}$ mil mylar. This source was put between two discs of 99.9999% Al which were 5/16" in diameter and 7 mils thick to form a sandwich. The entire sandwich was contained by a 1/2" × 3/32" × 20 mil pyrophollite ring and placed between 1/2" Bridgman anvils (Fig. 25). Two inch NaI detectors with lead slits 1-1/2" high and 20 mils wide were used; the slits were cut in lead blocks 2" thick and sufficiently large to cover the entire face of the detectors. The detectors were located 1 meter from the source. The slits were perpendicular to the plane of the sample so that the apparent size of the sample was independent of the angle between the detectors.

The positron source was calibrated initially. It was assumed that pressure changes in the annihilation spectrum of the source were small in comparison to the total pressure change in the spectrum and possible changes in the source spectrum were neglected in analyzing the data. The total annihilation spectrum at zero pressure and the calibration annihilation spectrum of the source are shown in Fig. 26. The source contributes roughly one-third of the total spectrum.

Annihilation spectra were taken at 0, 27, 54, 81, and 108 kbars. The pressure calibration was based on the phase transitions of bismuth in the same geometry using silver chloride as the pressure transmitter. In going from 0 to 100 kbars, the γ emission rate of the source was found to decrease by 20%; this was not surprising as in Mössbauer studies to 100 kbars the intensities of the Fe^{57} lines have been found to decrease as much as 80% because of deformation of the anvils;[72]

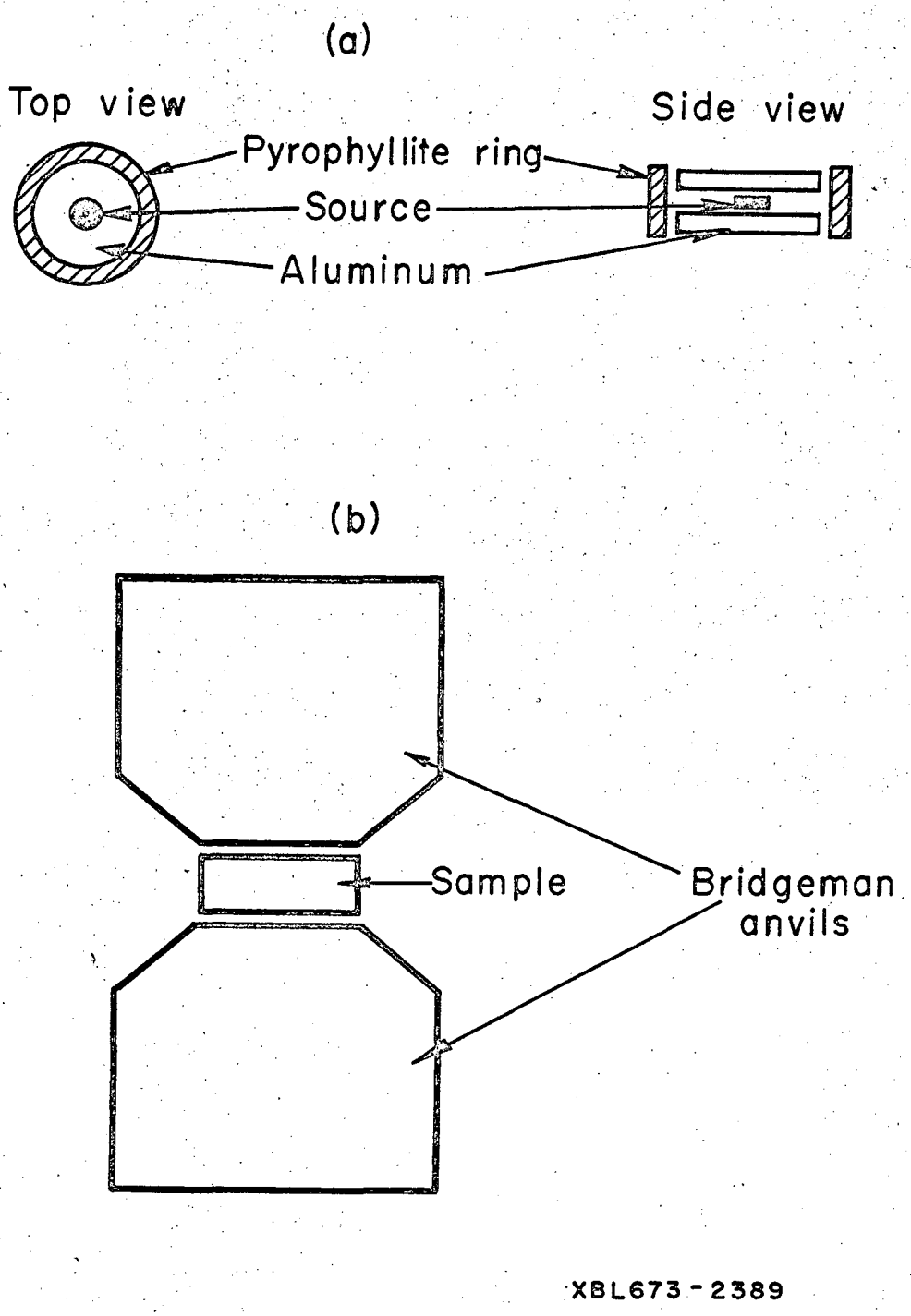

Fig. 25 The sample (a), source, metal, and containing ring is place between Bridgman anvils (b).

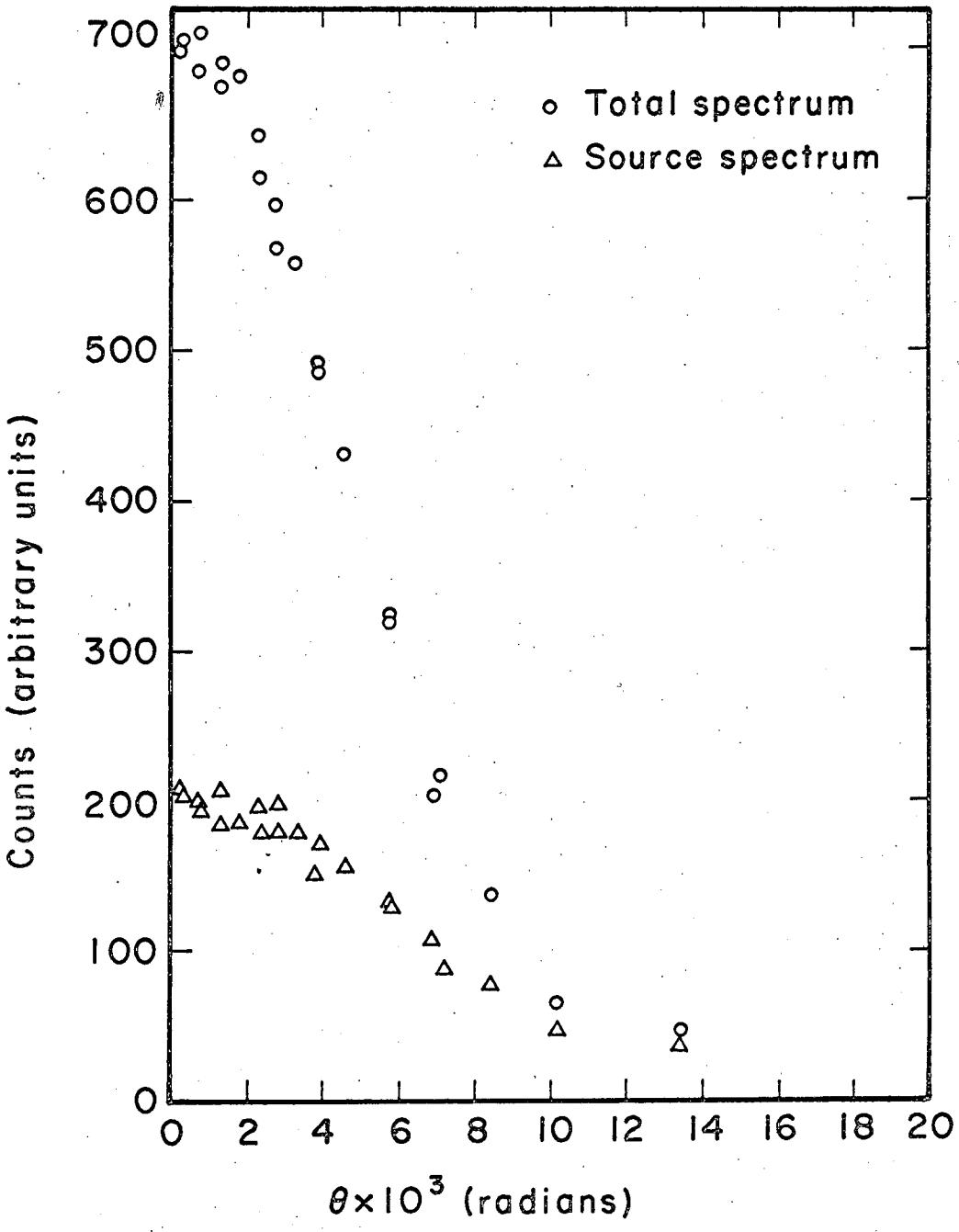

XBL 674-1396

Fig. 26 The total positron spectrum at 0 kb and the source calibration spectrum.

radiographs of the anvils have shown great deformation at 100 kbars. The raw data at each pressure were corrected for the pressure and time decrease in count rate. The aluminum spectrum at each pressure was obtained by subtracting the source spectrum from the corrected data assuming that the ratio of total source to total aluminum counts was constant over the pressure range of interest and that the shape of the source spectrum did not vary with pressure. The results for the Fermi momentum at each pressure did not depend greatly on these two assumptions.

D. Results

The positron annihilation spectrum of aluminum should be a central parabola with a tail at large angles. By fitting a parabola to the data at small angles we can obtain the Fermi momentum. If the source of the γ's is a point source and the resolution of the experimental apparatus is a delta function, the parabolic region of the experimental data should be fit by the parabola

$$N(\theta) = A - B\theta^2$$

where $N(\theta)$ is the number of counts per unit time at angle θ. Unfortunately the resolution of the apparatus is not a delta function and the source of γ's is not a point source.

The resolution for slits such as those used has been determined experimentally[65] and is shown in Fig. 27; Δ is the angular width of the lead slit, 5×10^{-4} radians. In order to estimate the error introduced by ths slit width we have replaced the experimental resolution by a square well (Fig. 27). Assuming a square resolution function, the count at angle θ is

$$N(\theta) = A\Delta^2 - B\Delta^2\theta^2 + \frac{1}{2} B\Delta^4$$

$$= A^* - B^*\theta^2 + \frac{1}{2} B^*\Delta^2$$

if $|\theta|$ is less than $\theta_F - \Delta$, where θ_F is the angle at which the parabola extrapolates to zero. The above expression for $N(\theta)$ is parabolic in θ.

For perfect slits of zero width the angle at which the central parabola extrapolates to zero, θ_F, corresponds to the Fermi momentum

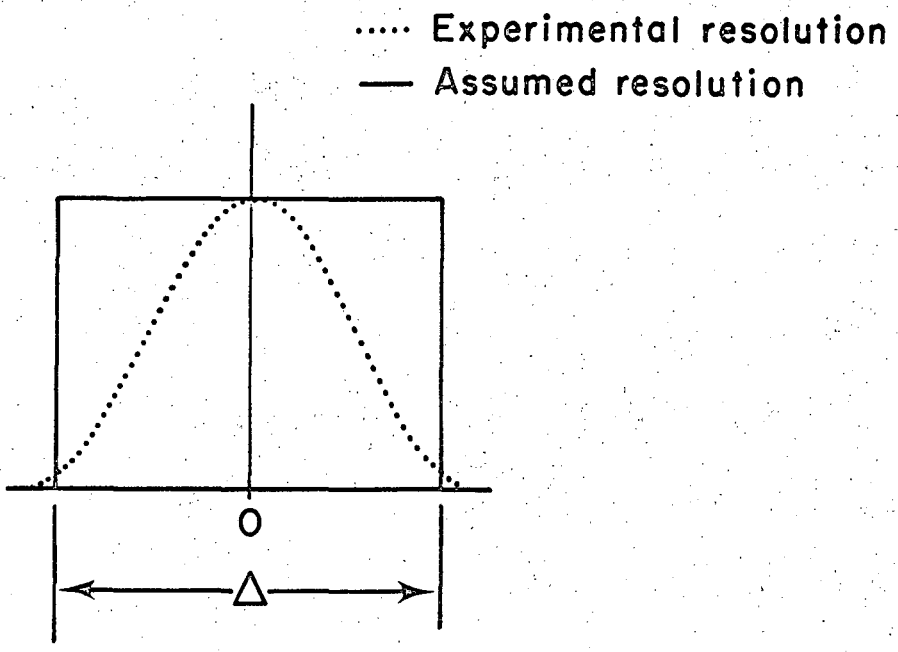

XBL 674-1401

Fig. 27 The experimental resolution of the slits[63] and that assumed for calculating error introduced by finite resolution. Δ is the angular width of the slits.

$$\theta_F = \left(\frac{A}{B}\right)^{1/2}$$

The 0 kbar data (Fig. 28) were fit with a parabola without using experimental points near θ_F. Assuming delta function slits gives

$$\theta_F = 6.79\times10^{-3} \text{ radians.}$$

For the assumed square resolution the fitting parabola is the same but the true Fermi angle is

$$\theta_F = \left(\frac{A^*}{B^*}\right)^{1/2} = 6.78\times10^{-3} \text{ radians}$$

rather than the angle at which the parabola extrapolates to zero. The error (~.2%) introduced by neglecting the corrections for the finite width of the lead slits is negligible compared with the statistical error in the experiments, ±1%. As the true resolution function is closer to a delta function than that assumed (Fig. 27) we may conclude that any errors due to the finite slit resolution are neglectable.

The true source of the γ's is not a point but rather a disk of less than 1/8" diameter; the source distribution on this disk is approximately uniform. Again we need only an estimate of the error due to the finite source. If we assume that the source is uniformly distributed on a line of length 1/8" (3×10^{-3} radians), we greatly overestimate any errors in our results. The difference between the Fermi angle, θ_F, calculated assuming a point source and assuming the above linear source distribution is a great overestimate of the true error and is less than .5% as long as no data points within 3×10^{-3} radians θ_F are used in fitting the parabola. The error introduced by the unknown source distribution is less than the statistical

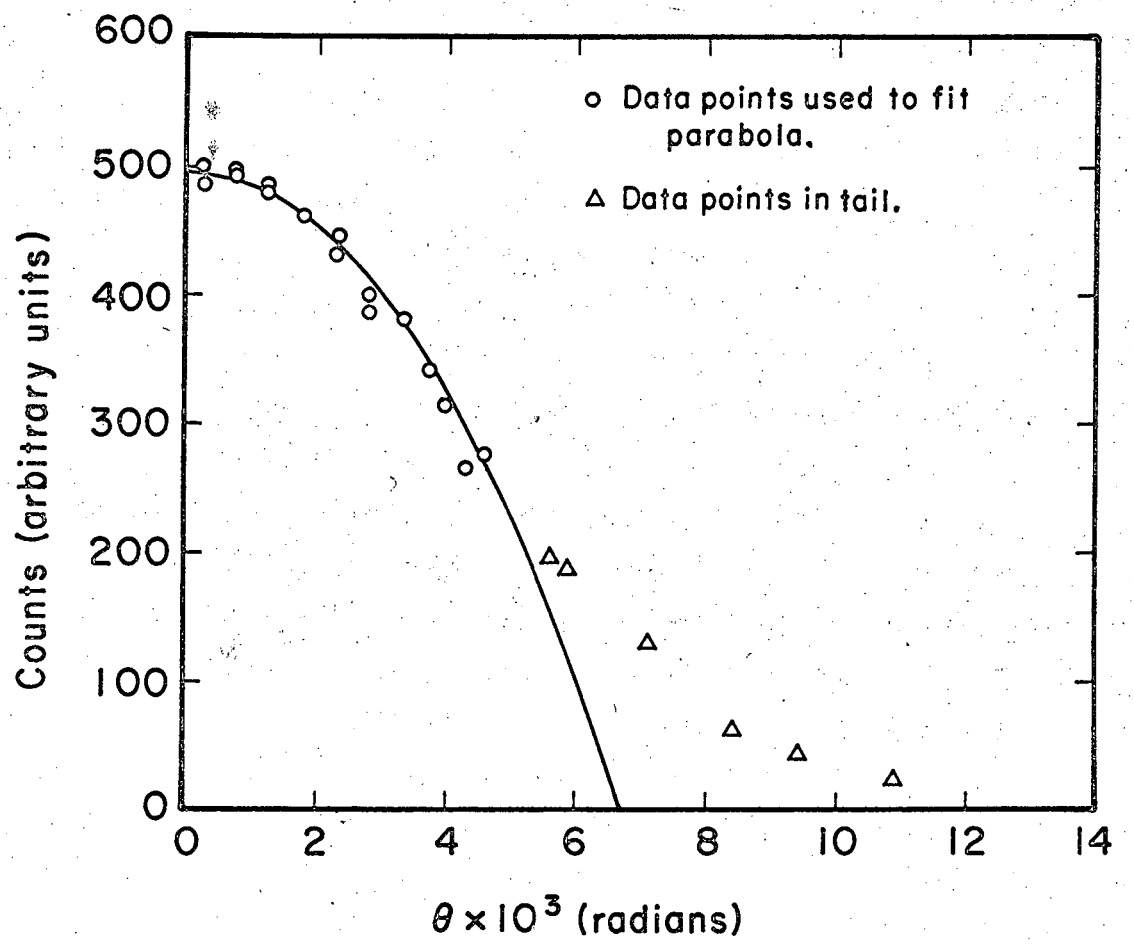

XBL 674-1390

Fig. 28 The 0 kbar positron annihilation spectrum of aluminum and the fitting parabola.

error in the experiment (± 1%). No data points within 2×10^{-3} radians of θ_F were used in fitting the parabola (Fig. 28); the source distribution error is neglected in evaluating the results as the above error estimate is a generous over-estimate.

At each pressure studied, the central protion of the observed annihilation spectrum of aluminum was fit. The data at 0 kbars and the fitting parabola are plotted in Fig. 28. The 0 kbar Fermi momentum is in excellent agreement with previous experimental work (Table XX). The Fermi momenta at the five pressures examined are plotted in Fig.29 as a function of pressure. The line in this figure is the Fermi momentum curve predicted by the free electron model

$$p_F = \hbar \left(\frac{3\pi^2 Z}{V} \right)^{1/3}$$

assuming three free electrons per atom and using the volume data for aluminum of Bridgman[72] and Jamieson.[73] The total observed change in the Fermi momentum was 3% and the errors on each of the five experimental Fermi momenta were ±1%. All of the data points lie within 1% of the theoretical curve. Figure 29 shows that the Fermi momentum of aluminum is very accurately described by the free electron model within the errors of this experiment.

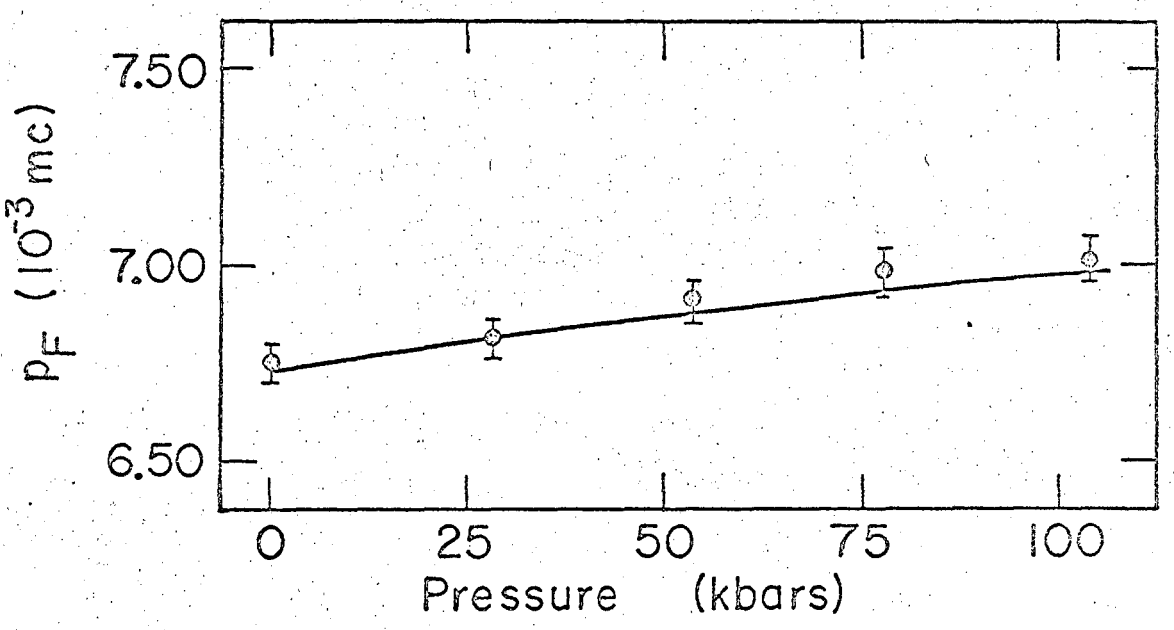

XBL673-2390

Fig. 29 The experimental Fermi momenta of aluminum as a function of pressure. The solid line is computed from the free electron model.

E. Discussion

We have found that the Fermi momentum of aluminum to 100 kbars is very accurately described by the free electron model. This is intuitively reasonable as the Fermi surface of aluminum at zero pressure is fairly close to that predicted by the free electron model assuming three electrons per atom. We would not expect the number of free electrons to increase with pressure as this would involve stripping core electrons off the aluminum ions which is energetically unfavorable.

Ashcroft[67] has shown that the zero pressure Fermi surface of aluminum can be fitted with two Fourier coefficients of a weak pseudo-potential in an OPW like calculation. Ashcroft assumed that the energy as a function of $\underline{k}$ was a constant on either side of a zone boundary instead of exhibiting the curvature predicted by the nearly free electron model (Fig. 30). In expressing the energy as a function of $\underline{k}$ he took into consideration the degeneracy of the energy bands close to more than one zone boundary. Ashcroft found that the shape of the Fermi surface in the third zone was strongly dependent on the values of the pseudo-potential coefficients and that the best fit to existing experimental data was obtained with

$$V_{111} = .0179 \text{ Ry}$$

$$V_{200} = .0562 \text{ Ry}$$

(compared with a Fermi energy of .856 Ry assuming an electron effective mass equal to that of a free electron). The shape of the Fermi surface in the second zone is not strongly dependent on the choice of the coefficients.

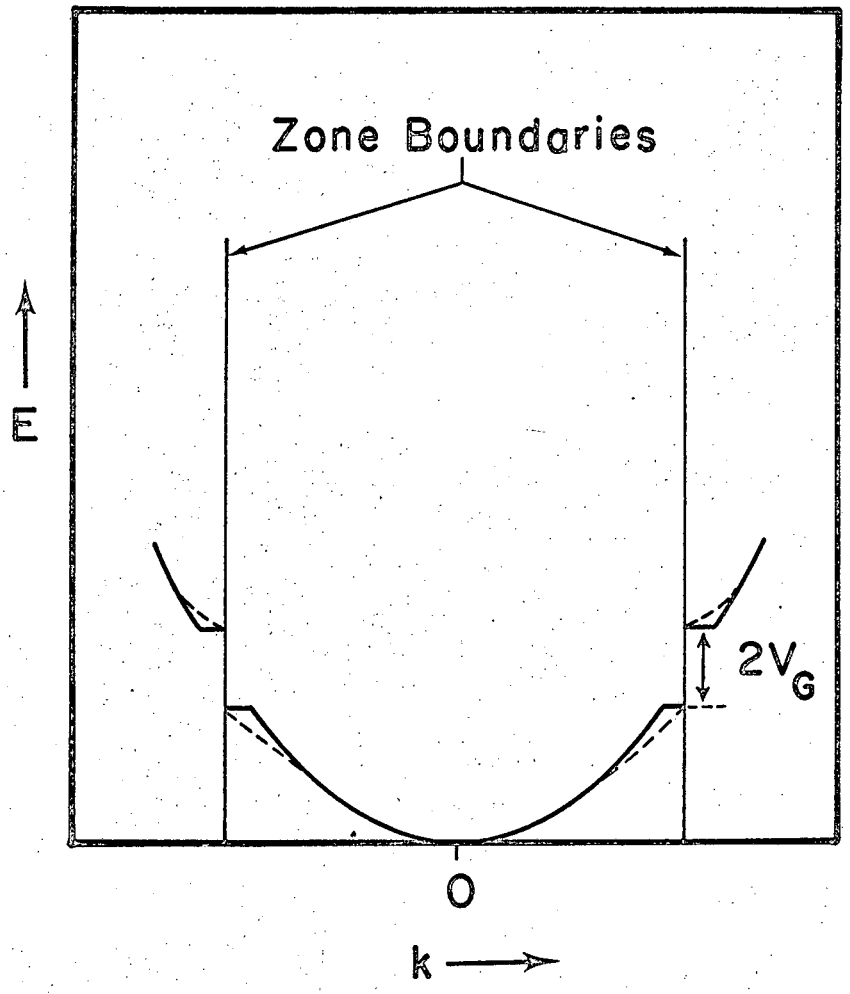

XBL 674-1391

Fig. 30 The electron energy as a function of $\underline{k}$. The solid line is that assumed by Ashcroft[67] and the dotted line is the predictions of the nearly free electron mode. V_G is the Fourier coefficient of the weak pseudo-potential appropriate to the zone boundary.

Melz[59] has found in experiments to 7 kbars that the Fermi surface of aluminum does not grow isotropically as would be expected if the band gaps were pressure independent. Using form factors proposed by Harrison[68] Melz obtained the pressure derivatives of the pseudo-potential coefficients

$$\frac{dV_{111}}{dP} = 1.6\times10^{-4} \text{ Ry/kbar}$$

$$\frac{dV_{200}}{dP} = 2.1\times10^{-4} \text{ Ry/kbar}$$

He found that these pressure derivatives adequately explained his data.

We have used the techniques developed by Ashcroft[67] to calculate the average momentum at the Fermi surface assuming the pressure derivatives of the pseudo-potential coefficients used by Melz to explain his results. In this calculation, we examined 1/48th of the unit cell in $\underline{k}$ space; the remainder of the unit cell was generated by its symmetry. This small portion of the cell was divided into one thousand prisms. For given values of the coefficients we assumed a value for the Fermi energy and found the volume enclosed by the surface of this energy by computing the volume enclosed in each prism. The value of the Fermi energy was then adjusted until the volume enclosed by the Fermi surface contained exactly three electrons. The Fermi momentum is the average momentum at the Fermi surface obtained in this way. The detailed shape of the third zone Fermi surface is strongly dependent on the choices of the pseudo-potential coefficients; however very little of the Fermi surface lies in the third zone. Therefore the average momentum at the Fermi surface, the Fermi momentum, does not depend greatly on the choice of coefficients.

We have computed the Fermi momentum at a number of pressures from 0 to 100 kbars assuming the pressure derivatives used by Melz and assuming that the coefficients are linear in pressure. Over the entire range of pressure the Fermi momenta calculated in this way were in close agreement with the values predicted by the free electron model. At 100 kbars, where the difference between the calculated and free electron values were the greatest, the free electron model predicts a Fermi momentum of 6.976×10^{-3} mc and, with the assumptions made for the pseudo-potential coefficients, we have obtained a Fermi momentum of 6.979×10^{-3} mc; the difference in these values is much smaller than the accuracy of the experiment, ±1%.

Within the accuracy of this experiment the Fermi momentum of aluminum to 108 kbars is in excellent agreement with the predictions of the free electron model. This result is not in disagreement with the work of Melz[67] to 7 kbars; Melz found that the detailed shape of the third zone Fermi surface is not explained by the free electron model and used pressure dependent band gaps to explain his results. However the average electron momentum at the Fermi surface which is all that can be obtained by these techniques does not depend strongly on the band gaps so long as they are small.

F. Conclusions

Utilizing positron annihilation we have found that the pressure dependence of the Fermi momentum of aluminum is accurately described by the free electron model. This suggests that positron annihilation studies of Fermi momenta may be an excellent tool for investigating either the pressure dependence of the volume of free electron metals or the high pressure electronic properties of metals for which the pressure dependence of the volume is well established. Positron annihilation would be most useful for studying metals with a large compressibility because of the difficulties involved in getting sufficient accuracy in the data and the weak expected volume dependence of the results.

ACKNOWLEDGMENTS

The author wishes to thank Professor George Jura for his constant supervision, guidance, and encouragement during the course of this work. He also wishes to thank Drs. B. J. Alder, A. Portis, and G. Somorjai for their helpful discussions of the work and is grateful to D. Newhart for his regular encouragement to work on theoretical problems. The author expresses his gratitude to Dr. W. Stark and Mr. J. Pryzbylinski for their regular noon time discussions which stimulated much of this work.

This work was supported by the United States Atomic Energy Commission.

References

1. I. Newton, Principia, Book II (1686).
2. A. Einstein, Ann. Physik 23, 183 (1907).
3. P. Debye, Ann. Physik 39, 789 (1912).
4. C. W. Garland and G. Jura, J. Chem. Phys. 22, 1108 (1954).
5. C. W. Garland and G. Jura, J. Chem. Phys. 22, 1114 (1954).
6. W. van Gool, Principles of Defect Chemistry of Crystalline Solids (Academic Press, New York, New York 1966).
7. I. M. Lifshitz, J. Phys. USSR 8, 89 (1944).
8. I. M. Lifshitz and L. N. Rosenzweig, Zh. Eksperim. i Teor. Fiz. 18, 1012 (1948).
9. R. F. Wallis, Phys. Rev. 105, 540 (1957).
10. A. A. Maradudin and R. F. Wallis, Phys. Rev. 148, 945 (1966).
11. R. Shuttleworth, Proc. Roy. Soc. (London) A62, 167 (1949).
12. B. J. Alder, J. R. Vaisnys, and G. Jura, J. Phys. Chem. Solids 11, 182 (1959).
13. L. A. Girifalco and V. G. Weizer, J. Phys. Chem. Solids 12, 260 (1960).
14. F. van Zeggeren and G. C. Benson, Can. J. Phys. 34, 985 (1956).
15. T. Kihara, J. Phys. Soc. Japan 3, 265 (1948).
16. B. J. Alder and M. van Thiel, Physics Letters 7, 317 (1963).
17. L. Jansen, Phys. Rev. A135, 1292 (1964).
18. H. J. Sparnaay, Physica 25, 217 (1959).
19. J. C. Rossi and F. Danon, J. Phys. Chem. Solids 26, 1093 (1965).
20. R. Bullough, H. R. Clyde, and J. A. Venables, Phys. Rev. Letters 17, 249 (1966).
21. B. J. Alder and R. H. Paulson, J. Phys. Chem. 43, 4172 (1965).
22. B. J. Alder, private communication.

23. J. E. Jones and A. E. Ingham, Proc. Roy. Soc. (London) A107, 636 (1925).

24. Ya. A. Kraftmakher and P. G. Strelkov, Soviet Physics - Solid State 8, 838 (1966).

25. H. Kanzaki, J. Phys. Chem. Solids 2, 24 (1957).

26. G. L. Hall, J. Phys. Chem. Solids 3, 210 (1957).

27. H. R. Glyde, J. Phys. Chem. Solids 27, 1659 (1966).

28. G. F. Nardelli and A. Repanai-Chiarotti, Nuovo Cimento 18, 1053 (1960).

29. A. J. E. Foreman and A. B. Lidiard, Phil. Mag. 8, 97 (1963).

30. L. A. Girifalco and J. R. Streetman, J. Phys. Chem. Solids 4, 182 (1958).

31. K. F. Stripp and J. G. Kirkwood, J. Chem. Phys. 22, 1579 (1954).

32. R. H. Johnson, J. Phys. Chem. Solids 26, 75 (1965).

33. F. A. Kroger and H. J. Vink, Solid State Physics, Vol. 3 (Academic Press, New York, New York), p. 307.

34. H. B. Huntington, Phys. Rev. 61, 325 (1945).

35. H. B. Huntington and F. Seitz, Phys. Rev. 76, 1728 (1949).

36. F. H. Brooks in Impurities and Imperfections (Am. Soc. for Metals, Cleveland, Ohio, 1955).

37. R. Fieschi, G. F. Nardelli, and A. Repanai-Chiarotti, Phys. Rev. 123, 141 (1961).

38. G. Boato, NASA Doc. N63-20074.

39. D. Lazarus, Solid State Physics, Vol. 10 (Academic Press, New York, New York), p. 71.

40. G. B. Gibbs, D. Graham, and D. H. Tomlin, Phil. Mag. 2, 1269 (1963).

41. R. F. Peart, J. Phys. Chem. Solids 26, 1853 (1965).

42. R. E. Howard and A. B. Lidiard, Reports on Progress in Physics 27, 161 (1964).

43. K. Mukherjee, Phil. Mag. 12, 915 (1965).

44. R. E. Hoffman, F. W. Pickus, and R. A. Ward, Trans. AIME 206, 483 (1956).

45. B. F. Dyson, T. Anthony, and D. Turnbull, J. Appl. Phys. 37, 2370 (1966).

46. A. Ascoli, B. Bollani, G. Gvarini, and D. Kustudic, Phys. Rev. 141, 732 (1966).

47. A. Kuper, H. Ketaw Jr., L. Slifkin, E. Sonder, and D. T. Tomizuka, Phys. Rev. 96, 1224 (1954).

48. C. T. Tomizuka, quoted in 39.

49. N. L. Peterson, Phys. Rev. 132, 2471 (1963).

50. C. T. Tomizuka and E. Sonder, Phys. Rev. 103, 1182 (1956).

51. A. Sawatzky and F. E. Jaumot Jr., J. Metals 9, 1207 (1957).

52. D. G. Gazis and R. F. Wallis, Surf. Sci. 3, 19 (1964).

53. L. A. Girifalco and V. G. Weizer, Phys. Rev. 114, 687 (1959).

54. J. E. Hove, Phys. Rev. 99, 430 (1955).

55. J. M. Blakely and Che-Yu Li, J. Phys. Chem. Solids 26, 1863 (1965).

56. B. Lax, Rev. Mod. Phys. 30, 122 (1958).

57. D. Caroline and J. E. Schirber, Phil. Mag. 8, 71 (1963).

58. P. R. Wallace, Solid State Physics, Vol. 10 (Academic Press, New York, New York, 1960), p. 1.

59. P. J. Melz, Phys. Rev. 152, 40 (1966).

60. D. Pines, Elementary Excitations in Solids (W. A. Benjamin, Inc., New York, New York, 1963).

61. J. M. Ziman, Electrons in Metals (Taylor and Francis Ltd., London, England, 1962).

62. J. M. Ziman, Principles of the Theory of Solids (Cambridge University Press, Cambridge, England, 1964).

63. G. Lang and S. De Benedetti, Phys. Rev. 108, 914 (1957).

64. J. M. Luttinger, Phys. Rev. 119, 1153 (1960).

65. F. Seitz, Modern Theory of Solids, (McGraw-Hill Book Co., New York, 1940).

66. W. A. Harrison, Phys. Rev. 116, 555 (1959).

67. N. W. Ashcroft, Phil. Mag. 8, 2055 (1963).

68. W. A. Harrison, Phys. Rev. 131, 2433 (1963).

69. G. E. Lee-Whiting, Phys. Rev. 97, 1557 (1955).

70. S. M. Kim, A. T. Stewart, and J. P. Carbotte, Phys. Rev. Letters 18, 385 (1967).

71. D. L. Raimondi, private communication.

72. P. W. Bridgman, Proc. Am. Acad. Arts Sci. 76, 55 (1948).

73. J. C. Jamieson, High Pressure Measurement (Butterworth's, Washington, D. C., 1963), p. 389.